Published online 2 July 2019

Nucleic Acids Research, 2019, Vol. 47, No. 15 ***8301–8317***
doi: 10.1093/nar/gkz571

Role of Era in assembly and homeostasis of the ribosomal small subunit

Aida Razi[1], Joseph H. Davis[2,3,4,†], Yumeng Hao[5,†], Dushyant Jahagirdar[1,†], Brett Thurlow[6], Kaustuv Basu[1], Nikhil Jain[7,8], Josue Gomez-Blanco[1], Robert A. Britton[7,8], Javier Vargas[1], Alba Guarné[9], Sarah A. Woodson[5], James R. Williamson[2,3] and Joaquin Ortega[1,*]

[1]Department of Anatomy and Cell Biology, McGill University, Montreal, Quebec H3A 0C7, Canada, [2]Department of Molecular Biology, The Scripps Research Institute, La Jolla, CA 92037, USA, [3]Department of Chemistry and The Skaggs Institute for Chemical Biology, The Scripps Research Institute, La Jolla, CA 92037, USA, [4]Department of Biology, Massachusetts Institute of Technology, Cambridge, MA 02139, USA, [5]T.C. Jenkins Department of Biophysics, Johns Hopkins University, Baltimore, MD 21218, USA, [6]Department of Biochemistry and Biomedical Sciences, McMaster University, Hamilton, Ontario L8S4K1, Canada, [7]Department of Molecular Virology and Microbiology, Baylor College of Medicine,Houston, TX 77030, USA, [8]Center for Metagenomics and Microbiome Research, Baylor College of Medicine, Houston, TX 77030, USA and [9]Department of Biochemistry, McGill University, Montreal, Quebec H3G 0B1 Canada

Received March 07, 2019; Revised June 11, 2019; Editorial Decision June 19, 2019; Accepted June 27, 2019

ABSTRACT

Assembly factors provide speed and directionality to the maturation process of the 30S subunit in bacteria. To gain a more precise understanding of how these proteins mediate 30S maturation, it is important to expand on studies of 30S assembly intermediates purified from bacterial strains lacking particular maturation factors. To reveal the role of the essential protein Era in the assembly of the 30S ribosomal subunit, we analyzed assembly intermediates that accumulated in Era-depleted *Escherichia coli* cells using quantitative mass spectrometry, high resolution cryo-electron microscopy and in-cell footprinting. Our combined approach allowed for visualization of the small subunit as it assembled and revealed that with the exception of key helices in the platform domain, all other 16S rRNA domains fold even in the absence of Era. Notably, the maturing particles did not stall while waiting for the platform domain to mature and instead re-routed their folding pathway to enable concerted maturation of other structural motifs spanning multiple rRNA domains. We also found that binding of Era to the mature 30S subunit destabilized helix 44 and the decoding center preventing binding of YjeQ, another assembly factor. This work establishes Era's role in ribosome assembly and suggests new roles in maintaining ribosome homeostasis.

INTRODUCTION

The bacterial 70S ribosome is made of the small (30S) and large (50S) subunits and consists of over fifty different ribosomal proteins (r-proteins) and ribosomal RNA (rRNA) that must fold and associate. During this assembly, the 16S rRNA in the 30S subunit and the 23S and 5S rRNA molecules in the 50S subunit fold according to energy landscapes comprised of multiple parallel assembly pathways (1,2). *In vivo*, ribosome biogenesis is aided by subunit-specific protein assembly factors that enable rapid (∼2 min) and efficient ribosome biogenesis (3). Although the specific function of most of these assembly factors is still unclear, they are generally thought to act by binding to the maturing particles and modifying their energy landscapes to favor folding pathways and to prevent the rRNA from falling into local energy minima (2).

The ribosome assembly factor Era (*Escherichia coli* Ras-like) is known to participate in 30S subunit maturation; however, its precise role is still largely unknown. This protein is universally conserved in both eukaryotes and prokaryotes (4) and it is essential for both Gram-negative (5–7) and Gram-positive bacteria (8,9). Era is comprised of a N-terminal GTPase domain and a C-terminal KH (K-homologue) domain connected by a 17 amino acid long flexible linker whose length is important for its function

*To whom correspondence should be addressed. Tel: +15 1439 85230; Email: joaquin.ortega@mcgill.ca
†The authors wish it to be known that, in their opinion, the second, third and fourth authors should be regarded as Joint Second Authors.

(10). The GTPase domain consists of a central β-sheet flanked by five helices. The KH domain has a high structural similarity to the RbfA assembly factor and folds following a type 2 (αββααβ) KH folding pattern. This KH domain is necessary for Era to bind the 16S rRNA and the 30S subunit (11,12).

Crystallography studies with purified Era and RNA fragments derived from the 3′ end of the 16S rRNA (13) revealed that the two domains of Era can adopt a 'closed' and an 'open' conformation. In the apo or GDP-bound states, Era adopts the open conformation in which the nucleotide binding site is accessible but the RNA binding site in the KH domain is occluded. Binding of GTP is thought to drive Era to the closed state, thus allowing for rRNA binding (13–15). According to this model, subsequent rRNA binding, which is known to stimulate GTP hydrolysis (13), would then revert Era to the open state and trigger release of Era from the rRNA. These findings are consistent with equilibrium binding assays in which Era exhibited increased affinity for rRNA in the presence of GDPNP, a non-hydrolyzable GTP mimic, relative to that in the presence of GDP (16,17).

Although binding to the isolated rRNA fragment can be modeled by this two-state conformational switch model, Era may adopt additional conformations when bound to entire 30S subunit. Indeed, a low resolution cryo-electron microscopy (cryo-EM) structure of Era in complex with the 30S subunit found that neither of the aforementioned conformations were compatible with the orientation of the two domains of Era when the factor was bound to the cleft region between the head and platform on the 30S subunit (18).

To determine the role of Era in the 30S subunit assembly, we employed quantitative mass spectrometry (qMS), high-resolution cryo-electron microscopy (cryo-EM) and in-cell footprinting to analyze 30S subunit assembly intermediates ($30S_{Era\text{-}depleted}$ particles) that accumulated in *E. coli* under Era depletion conditions. In addition, we investigated a potential role of Era in ribosomal quality control and we further explored the functional interplay between Era and another assembly factor, YjeQ (19).

Here, we found that in the absence of Era, all of the major 16S rRNA domains fold correctly with the exception of helices 23 and 24 in the platform region, suggesting that maturation of these helices directly or indirectly relies on Era. Notably, our structures indicate that the assembling particles did not stall at the maturation step folding helices 23 and 24. Instead, particles skipped the folding of these two helices and were re-routed in their folding pathway to continue the maturation of other structural motifs. This analysis suggests that assembly of the 30S subunit is not necessarily sequential (from 5′ to 3′) and that at least in the absence of Era, all three major domains of the 16S rRNA can co-mature. Further, we found that treatment of mature 30S subunits with Era destabilizes functionally essential regions of the particle and inhibits binding of YjeQ. Overall, these results suggest that Era binds to the immature 30S subunit independently from YjeQ. The observed ability of Era to induce significant conformational changes in the mature 30S subunit also suggests new roles of this protein in ribosome homeostasis.

MATERIALS AND METHODS

Cell strains and protein overexpression clones

The parental *E. coli* K-12 (BW25113) strain was obtained from the Keio collection, a set of *E. coli* K-12 in-frame, single gene knockout mutants (20).

The pET15b-*era* plasmids used for overexpression of Era were produced as described (17). The pDEST17-yjeQ plasmid used to overexpress YjeQ protein with an amino-terminal His_6 tag cleavable by tobacco etch virus (TEV) protease was generated as described previously (21).

Protein expression and purification

Overexpression and purification of Era (17) and YjeQ (22) proteins were done as previously described.

Creation of the Era-depleted strain

To generate the essential *era* gene depletion strain in the BW25113 *E. coli* background, we used the previously described pBS-*araBAD*flank*kan* plasmid (23) and the temperature sensitive pSim6 plasmid (24) for insertion of *era* at the *araBAD* locus and recombination into the chromosome, respectively. PCR amplification of the *era* gene was performed with the Era_up-R and Era_down-F oligonucleotides (Supplementary Table S2) using the previously described pET15b-*era* plasmid (17) as a template for amplification. The amplified product was cloned into the *PmeI* site of the pBS-*araBAD*flank*kan* and the resulting plasmid with *era* in the forward orientation with respect to the *araBAD* promoter was sequenced and named 'pBS-*araBAD*flank*erakan*'. The *era* knockout cassette was generated by PCR amplification of pSET152 (25) with the Era_Apra-F and Era_Apra-R oligonucleotides (Supplementary Table S2). This generated an ∼1100 bp product that contained the apramycin^r cassette flanked by 50 bp of the upstream and downstream sequences of the native *era* gene.

The precise deletion of *era* was carried out as described by (26,27). pBS-*araBAD*flank*erakan* was double digested with *NotI* and *PsiI* resulting in an ∼3200-bp and 2600-bp product. The digestion reaction was resolved in a 1% agarose gel and the 3.2 kb product containing the *era* gene flanked by homologous regions to the *araBAD* promoter was excised and gel purified using the QIAquick gel extraction kit (Qiagen). Approximately 100 ng of this product was used to transform BW25113-pSim6 competent cells using electroporation and cells were plated on LB-agar containing 50 μg/ml kanamycin at 37°C overnight to select for integrants at *araBAD* and facilitate curing of the temperature-sensitive pSim6 plasmid. To screen for strains in which the *araBAD* genes had been replaced by *era*, genomic DNA was isolated from the clones and used as a template for PCR amplification with the Era_down-F and Ara_up-R oligonucleotides (Supplementary Table S2 and Supplementary Figure S1A; top panel). A second round of PCR screening was performed using the Ara_int-F and Kan_int-R oligonucelotides (Supplementary Table S2 and Supplementary Figure S1A;

bottom panel). A strain positive for chromosomal integration was selected and named '*araBAD-era*'. The *era* gene deletion protocol was conducted by transforming ∼100 ng of the *era* knockout cassette using electroporation into *araBAD-era*-pSim6 cells followed by plating onto LB-agar containing 50 μg/ml kanamycin and 100 μg/ml apramycin and overnight incubation at 37°C to select for integrants at the *era* locus and enable curing of the pSim6 plasmid. Genomic DNA was isolated from clones and used as a template for PCR amplification using the EraKO_confirm-R and Apra_int-F oligonucleotides (Supplementary Figure S1B; top panel) and the Apra_int-R and EraKO_confirm-F oligonucleotides (Supplementary Table S2 and Supplementary Figure S1B; bottom panel) were used to confirm the deletion of *era*. The resulting strain with genotype *araBAD*::*era-kan*^{r}, *era*::*apr*^{r} was called 'Era-depleted'.

Strain growth experiments

To obtain the growth curves for the parental and Era-depleted strains, the cultures were grown overnight in LB media at 37°C with shaking at 225 rpm in an Excella E24 incubator (New Brunswick). In the case of the Era-depleted strain, the LB media was supplemented with 1% arabinose. The overnight cultures were diluted 1/10 000 with LB media to a final volume of 100 μl in a 96-well plate with fresh LB media and the Era-depleted strain was grown in either the presence or absence of 1% arabinose. Cultures were incubated at either 37 or 15°C with shaking in a Tecan Sunrise™ Plate Reader for either 24 or 72 h, respectively. Culture density was monitored by measuring the optical density at 600 nm (OD_{600}) every 10 min during the time course of the experiment. Optical density was plotted over time (minutes) to show the growth curve for each strain at both 37 and 15°C. The experiment was performed with five replicates.

Dilution plating experiments were performed by inoculating 0.5 ml of a saturated overnight culture in 50 ml of fresh LB media. Cultures were grown at 37°C with shaking until an OD_{600} of 0.2. Then, serial dilutions were made in 10-fold increments, and 5 μl of each dilution was immediately spotted onto LB agar plates with and without 1% arabinose and incubated at 37°C. The plates were incubated for the same amount of time until isolated colonies of the parental strain reached ∼2 mm in diameter.

Purification of ribosomal particles from parental and Era-depleted strain

Purification of mature 30S subunits was done from the parental *E. coli* K-12 (BW25113) strain after 1 L of LB media were inoculated with 10 ml of saturated overnight culture and grown to an OD_{600} of 0.2. Cultures were then cooled down to 4°C and purification of the mature 30S subunits that were used in the cryo-EM experiments was done as previously described (22). In the case of the 30S subunits and 70S ribosomes purified under 'low salt' conditions for mass spectrometry, we used a previously published protocol (28), but all buffers A–E contained only 60 mM NH_4Cl. In addition, the salt wash performed with buffer C was omitted.

In the case of the $30S_{Era\text{-}depleted}$ particles and 70S ribosomes from Era-depleted strain, overnight cultures of this strain were grown at 37°C with shaking at 225 rpm in LB media containing 1% arabinose, 100 μg/ml apramycin and 50 μg/ml kanamycin. To initiate depletion, cells from saturated overnight cultures were pelleted by centrifugation at 12 000*g* in a microcentrifuge and all arabinose containing media were removed. Cells were then diluted to OD_{600} of 0.02 in LB media containing 100 μg/ml apramycin and 50 μg/ml kanamycin and grown at 37°C with agitation until they reached a doubling time of ∼150 min. Cells were not allowed to grow beyond an OD_{600} of 0.2, thus if at this point cells were still exhibiting doubling times <150 min, then the culture was diluted again to $OD_{600} = 0.02$ into pre-warmed LB media with the same apramycin and kanamycin but without arabinose. Typically, two cycles of growth dilution were required before the cells reached ∼150 min doubling time and then cultures were used to inoculate 4 L of pre-warmed media to an OD_{600} of 0.02 and cells were grown with agitation until they reached an OD_{600} of 0.2. Full depletion of the Era protein was obtained in cells with a doubling time of 225–275 min. At that point, cells were harvested for purification of $30S_{Era\text{-}depleted}$ particles and 70S ribosomes. To purify these particles, we used a similar protocol using ultracentrifugation over sucrose gradients as previously described (28). However, all buffers A–E contained only 60 mM NH_4Cl. In addition, the salt wash performed with buffer C was omitted. This purified $30S_{Era\text{-}depleted}$ particles and 70S ribosomes were used both for cryo-EM and mass spectrometry experiments. The calculation of the proportion of free 30S subunits in the Era-depletion strain from the sucrose gradient was done as previously described (17).

Ribosomal RNA analysis of Era-depleted and parental strains by qPCR

Quantitative real-time PCR (qPCR) was carried out using total RNA isolated from the parental and Era-depleted strain (grown under depletion conditions). The rRNA from each sample was purified using the RNeasy mini kit (Qiagen) according to the manufacturer's protocol. RNA concentration in the sample was then measured by A_{260}, where 1 absorbance unit is equivalent to 40 μg/ml of RNA. cDNA synthesis was carried out using 100 ng of random hexamer primers and 10 ng of total RNA with Superscript III reverse transcriptase (Invitrogen) by following manufacturer protocol. cDNA was amplified by primer set P1, P2 and P3 (Supplementary Table S3). ΔC_t values for P2 and P3 oligo sets amplification for both wild-type and Era-depleted strains were calculated against total 16S rRNA fragment measured by P1 set of oligos amplification. $\Delta\Delta C_t$ was calculated for ΔC_t (Era-depleted) − ΔC_t (wild-type) and fold expression was calculated by $2^{(-\Delta\Delta Ct)}$. Standard deviations were calculated as described in manufacturer protocol of applied biosystem.

Quantitative mass spectrometry

To analyze the ribosomal particles purified from Era-depleted and parental strains by qMS, we first generated ^{15}N-isotopically labeled isotopic reference standards by growing strain JD0189 (*E. coli* NCM3722 (29)) to OD_{600} 0.4 in ^{15}N-labeled minimal media at 37°C as described previously (30). Cells were pelleted and resuspended in 50 mM

Tris, 100 mM NH_4Cl, 10 mM $MgCl_2$, pH 7.8, to a concentration of 3.0 OD_{600} units/ml, which corresponds to ∼0.05 μM ribosomes, assuming 5 × 10^8 cells/OD_{600}/ml and 20,000 ribosomes/cell. ^{15}N-labeled 70S reference particles samples were generated by growing strain JD0189 to OD_{600} 0.7 in ^{15}N-labeled media as described above. Cells were lysed, and 70S particles were purified on a 10–40% sucrose gradient as described (30). Fractions bearing monosomes or polysomes were pooled and saved at −80°C at 0.055 μM.

To generate tryptic peptides, particles were isolated as described above and concentrated to 0.5 μM. To each sample (10 pmols), an equimolar ^{15}N-labeled spike sample (either purified ribosomal particles or lysate bearing ∼10 pmols of ribosomes) was added, mixed, and trichloroacetic acid (TCA) was added to 13% final concentration. After overnight precipitation at 4°C, pellets were sequentially washed with 10% TCA, 100% acetone and were dried before they were resuspended in 40 μl buffer B (100 mM NH_4CO_3, 5% acetonitrile, 5 mM dithiothreitol) as described (31). After reduction for 10 min at 65°C, cysteines were alkylated by addition of iodoacetamide to 10 mM and incubation at 30°C for 30 min. Then, 0.2 μg trypsin was added, and protein digestion proceeded at 37°C overnight. Tryptic peptides were purified on C18 PepClean columns, and ∼1 μg of peptides were mixed with 500 fmol iRT retention time standards (Pierce) and injected onto the LC/MS.

To perform qMS, peptides were trapped on a ChomXP C18 cHiPLC column (Sciex) and resolved on a 15 cm ChromXP C18 cHiPLC analytical column using a 120-min 5–35% linear acetonitrile gradient with a flow rate of 300 nl/min. Data were acquired in replicate with either data-dependent acquisitions or SWATH data-independent acquisition (DIA) mode. Briefly, data-dependent acquisitions included one MS1 scan (200 ms accumulation time) followed by 30 MS2 scans (100 ms accumulation time). The SWATH DIA method consisted of one MS1 scan (200 ms accumulation time) followed by 32 MS2 scans (25 m/z wide, 100 ms accumulation time) covering the range 400–1200.

To analyze the abundance of the r-proteins in the ribosomal particles, DDA datasets were searched with comet (32), peptide-spectra matches (PSM) were scored with PeptideProphet (33) and scored PSMs were combined with iProphet (34). A consensus spectral library was generated using Spectrast (35). Using this spectral library, a target list bearing ^{14}N- and ^{15}N-labeled precursor and product ions corresponding to ribosomal proteins of interest was generated using Skyline (36), and ion chromatograms were extracted in regions of the chromatogram near the predicted elution time as determined using the iRT standards (37). Extracted ion chromatograms were filtered for interfering ions at both the MS1 and MS2 levels, and relative peptide abundance was calculated as ^{14}N_total_area/^{15}N_total_area. For each sample and for each protein, the median peptide abundance ratio was then calculated, and these values were clustered across both samples and proteins using the ward linkage method and the Euclidean distance metric (38). Non-ribosomal proteins were analyzed as described using a spectral library focused on assembly co-factors (J. H. Davis, in preparation) (30).

In vivo DMS footprinting experiments

To prepare the cells for *in vivo* DMS footprinting, Era-depleted cells were grown overnight in LB supplemented with apramycin (100 μg/ml), kanamycin (50 μg /ml) and 1% arabinose at 37°C with shaking at 200 rpm. A 10 ml aliquot of this overnight culture was collected as the 'Era pre' sample to be used for *in vivo* DMS footprinting (see below). Fresh LB medium (150 ml) with apramycin (100 μg/ml) and kanamycin (50 μg/ml) were inoculated with 150 μl overnight culture to achieve an OD_{600} = 0.02. The culture was grown at 37°C until the doubling time reached 100–150 min. This culture was then used to inoculate fresh LB media without antibiotic (initial OD_{600} was 0.02). The culture was grown until the doubling time reached 200–250 min, when two 50 ml aliquots were removed as the Era depleted (Era-) samples. A portion of the Era depleted culture was sub-cultured to an OD_{600} of 0.02 into LB media with apramycin (100 μg/ml), kanamycin (50 μg/ml) and 1% arabinose to induce Era expression, and this time was recorded as the start of Era re-expression. About 50 ml of samples were collected for analysis and DMS footprinting at 1, 2, 3, 4 and 4.5 h after Era re-expression. As a control for second site suppressors, a portion of the Era- culture was re-diluted to an OD_{600} of 0.02 in LB without antibiotics or arabinose. The cultures containing arabinose had a shorter doubling time than the control sample lacking arabinose. During the entire procedure, the growth of all cultures was measured every hour to avoid exceeding an OD_{600} = 0.2, at which point cultures were diluted to OD_{600} = 0.02 with fresh medium.

The *in vivo* DMS footprinting was carried out on 50-ml cultures, OD_{600} = 0.2, by adding 5 ml 20% (v/v) dimethyl sulfate in ethanol at room temperature for 30 s. The methylation reaction was quenched with 25 ml of ice-cold 1.4 M β-mercaptoethanol and 25 ml of water-saturated isoamyl alcohol for 30 s on ice. The cells were collected at 4000 rpm (3,315 *g*) for 10 min using a JS-5.3 rotor (Beckman Coulter). The cell pellets were resuspended twice in the same volume of 0.7 M β-mercaptoethanol and harvested by centrifugation after each step. The washed pellets were stored at −80°C prior to RNA extraction.

Total RNA was extracted from each cell pellet using the RNeasy mini-prep (Qiagen), and the final RNA concentration was determined from the UV absorption. The DMS modification pattern was analyzed by reverse transcription as previously described (39,40). For each reaction, 2 μg total RNA was annealed with 2 pmol (30,000 cpm) ^{32}P-labeled primer (primer 46 or primer 812) (Supplementary Table S4) at 65°C for 3 min before extension with Superscript III (Thermo Scientific) for 60 min at 55°C. Sequencing lanes were normalized to the total intensity in each lane, excluding the unextended primer and the full-length cDNA, using ImageQuant software. This was followed by background subtraction of the control lanes (– DMS) in Microsoft Excel.

70S dissociation experiments

The parental *E. coli* K-12 strain (BW25113) was used for purification of the 70S ribosomes used in these experiments. Typically, 3 L of LB media were inoculated with 10 ml each

of saturated overnight culture and grown to an OD_{600} of 0.6. Cells were harvested by centrifugation at 3700 *g* for 15 min. Cell pellets were resuspended in 7 ml of buffer A (20 mM Tris-HCl at pH 7.5, 10 mM magnesium acetate, 100 mM NH_4Cl, 0.5 mM EDTA, 3 mM 2-mercaptoethanol), and a protease inhibitor mixture (cOmplete Protease Inhibitor Mixture Tablets; Roche) and DNaseI (Roche). Each of the subsequent steps was performed at 4°C. The cell suspension was passed through a French pressure cell at 1400 kg/cm^2 three consecutive times to lyse the cells. The lysate was spun at 59 000 *g* for 30 min to clear cell debris. Resulting supernatant was layered over a sucrose cushion of equal volume composed of 30% sucrose in buffer B (20 mM Tris-HCl, pH 7.5, 10 mM magnesium acetate, 500 mM NH_4Cl, 0.5 mM EDTA and 3 mM 2-mecaptoethanol), and then spun down for 4.5 h at 321 000 *g*. The pellet was resuspended in buffer C containing 10 mM Tris-HCl, pH 7.5, 10 mM magnesium acetate, 500 mM NH_4Cl, 0.5 mM EDTA and 3 mM 2-mecaptoethanol and then spun for 16 h at 100 000 *g*. The washed ribosome pellet was resuspended in buffer E containing 10 mM Tris-HCl, pH 7.5, 10 mM magnesium acetate, 60 mM NH_4Cl and 3 mM 2-mecaptoethanol, which caused subunits to be associated. Approximately 120 A260 units of resuspended crude ribosomes were then applied to 34 ml of 10–30% (wt/vol) sucrose gradients prepared with buffer E. The gradients were centrifuged for 16 h at 40 000 *g* on a Beckman Coulter SW32 Ti rotor. Gradients were fractionated using a Brandel fractionator apparatus and an AKTA Prime FPLC system (GE Healthcare). The elution profile was monitored by UV absorbance at A_{254}, and fractions corresponding to the 70S subunit peak were pooled and spin down for another 4.5 h at 321 000 *g* on a Beckman SW32 Ti rotor. The pellet was resuspended in Buffer E.

To perform the 70S dissociation experiment, purified Era was first passed through a Superdex 200 size-exclusion column (GE Healthcare) equilibrated with buffer containing 50 mM Tris-HCl, pH 8.0. To assemble the dissociation reaction, 1 μM 70S ribosomes were incubated with either 2- or 5-fold molar excess of Era. Reactions had a total volume of in a 120 μl and were assembled in buffer containing 20 mM Tris-HCl, pH 7.5, 20 mM magnesium acetate, 30 mM potassium chloride and 4 mM 2-mecaptoethanol. Where indicated we added up to 1 mM of nucleotide (GTP/GDP/GMPPNP). After 15-min incubation at 37°C, each reaction was loaded onto 34 ml 10–30% (wt/vol) sucrose gradients prepared with buffer E and centrifuged for 16 h at 40 000 *g* on a Beckman Coulter SW32 Ti rotor. Gradients were fractionated using a Brandel fractionator apparatus and an AKTA Prime FPLC system (GE Healthcare). The elution profile was monitored by UV absorbance at A_{254}.

Microscale thermophoresis

Mature 30S subunits were fluorescently labeled as described (17). Prior to each MST experiment, all samples were centrifuged at 14 000 *g* for 10 min to remove any aggregates. All reaction and titration series were prepared in MST buffer containing 20 mM Tris–HCl, pH 7.5, 150 mM NaCl, 10 mM $MgCl_2$, 1 mM DTT, 0.05% Tween-20, 0.4 mg/ml BSA and were incubated in 0.5 ml Protein LoBind eppendorf tubes. Prior to performing the MST experiment, 0.5 μM fluorescently labeled mature 30S subunits were incubated with either 5 or 10 μM Era. GMPPNP was added to a final concentration of 1 mM and the assembly reaction was incubated for 15 min at room temperature. A 1:1 serial dilution of non-labeled YjeQ was then prepared in MST buffer starting at 4 μM. The 30S+Era reaction mixtures were then diluted with MST buffer containing 1 mM GMPPNP until the 30S subunits reached a concentration of 40 nM. For the titration assay, 10 μl of the corresponding serial dilution of the non-labeled YjeQ was mixed with 10 μl of the fluorescently labeled 30S subunit pre-bound with Era (or without Era for the negative control). Titration reactions were then incubated for 10 min at room temperature loaded into premium capillaries (NanoTemper Technologies) and MST analysis was performed using the Monolith NT.115 (NanoTemper Technologies) at ambient temperature. An LED power of 100% and an MST power of 20–60% were used during MST readings. The resulting binding curves were obtained by plotting the normalized fluorescence (F_{norm} (%) $= F_1 / F_0$) versus the logarithm of YjeQ concentration. K_ds were calculated using the NanoTemper MO Affinity Analysis software v2.2.6. Experiments were performed in triplicates.

Cryo-electron microscopy

The $30S_{Era\text{-}depleted}$ particles were prepared for imaging with cryo-EM by preparing a dilution of the particles in buffer E (10 mM Tris-HCl at pH 7.5, 10 mM magnesium acetate, 60 mM NH_4Cl and 3 mM 2-mercaptoethanol) to a concentration of 30 nM that was applied directly to the grid and immediately right after the dilution step. The reactions containing 30S and Era for cryo-EM experiments were prepared as followed. A 20 μl reaction was first prepared in buffer E containing mature 30S subunits (0.5 μM) and Era protein (20 μM). GMPPNP was added to this reaction to a concentration of 2 mM. After the reaction was incubated at 37°C for 15 min, the reaction was diluted 5-fold in buffer E containing GMPPNP at 2 mM and free Era protein at 4 μM and immediately applied to the EM grid. Finally, in the reaction containing mature 30S, Era and YjeQ for cryo-EM experiments, these components were added to final concentrations of 2, 20 and 3.5 μM, respectively. GMPPNP was added to this reaction to a concentration of 2 mM. After the reaction was incubated at 37°C for 15 min, the assembly reaction was diluted 10-fold in buffer E containing GMPPNP at 2 mM and immediately applied to the EM grid.

In all samples, a volume of 3.6 μl of the diluted sample was applied to holey carbon grids (c-flat CF-2/2–2C-T) with an additional layer of continuous thin carbon (5–10 nm). Before the sample was applied, grids were glow discharged in air at 5 mA for 15 s. Vitrification of samples was performed in a Vitrobot (Thermo Fisher Scientific Inc.) by blotting the grids once for 3 s and with a blot force +1 before they were plunged into liquid ethane. The Vitrobot was set at 25°C and 100% relative humidity.

Automated data acquisition was performed using EPU software at FEMR-McGill using a Titan Krios microscope at 300 kV equipped with a Falcon II direct elec-

tron detector (Thermo Fisher Scientific Inc.). Movies for the $30S_{Era\text{-}depleted}$ particles, Era-treated 30S particles and Era+YjeQ-treated 30S particles were collected with a total dose of 35, 46 and 28 $e^-/Å^2$, respectively. All datasets were collected as movies with seven frames acquired in 1 s exposure at a magnification of 75 000×, producing images with a calibrated pixel size of 1.073 Å. The nominal defocus range used during data collection was between −1.25 and −2.75 μm.

Image processing

Motion correction and contrast transfer function (CTF) estimation for each collected movie were done with MotionCor2 (41) and Gctf (42) programs, respectively. From here all processing were done with Relion 2.1 program (43). Particle images after the autopicking process were subjected to reference-free 2D classification to produce a 'clean' dataset. The selected particles were subsequently used for hierarchical 3D classification approaches. The initial 3D reference used for these classifications was either a 60 Å low pass filtered map of the mature 30S subunit, the intermediate cryo-EM maps obtained during classification or maps obtained by *ab initio* approaches. The *ab initio* methodologies we used to generate these initial maps were random sample consensus (RANSAC) as implemented in Scipion (44) and common lines as implemented in EMAN2 (45). In the case of the 3D classifications of the datasets for the $30S_{Era\text{-}depleted}$ particles and the Era-treated 30S particles, no mask was used. However, masks created from the mature structure or intermediate maps obtained during the classification were used in the case of the Era+YjeQ-treated 30S particles. All masks were obtained with 'relion_mask_create' command using an initial threshold for binarization of 0.01, extension of the binary mask by two pixels and creating a soft-edges with a width of two pixels. Classes obtained at the end of each classification approach were inspected visually and those deemed to represent the same structures were grouped for refinement. A soft-mask was applied in all refinements.

To improve the details on the density potentially representing Era in the Era-treated 30S particles and Era+YjeQ-treated 30S particles, the corresponding datasets were subjected to focus classification with subtraction of the residual signal using Relion (46), following an approach previously described (47).

Sharpening of the cryo-EM maps was done by applying a negative B-factor estimated using automated procedures (48). Local resolution analysis of the structures was also done using Relion procedures (43).

Map analysis and atomic model building

Visualization of the cryo-EM maps was done using Chimera (49). Before initiating high-resolution model building of the cryo-EM map obtained for the $30S_{Era\text{-}depleted}$ particle (class P), we maximize detail and connectivity of this map using the automatic sharpening tool phenix.auto_sharpen (50), which is available as part of the PHENIX software suite (51). The starting point for the modeling of this map was the atomic model of the mature 30S subunit (PDB ID: 2AVY). This initial model was first fit into the density as a rigid body using Chimera (49) and the final model was built with successive rounds of real space refinement in Phenix (52) and manual model building in Coot (53,54). Areas of the map not exhibiting corresponding density were deleted and not incorporated into the models.

Figures for this manuscript were prepared using Pymol program (The PyMOL Molecular Graphics System, Version 1.2r3pre, Schrödinger, LLC), UCSF Chimera and Chimera X (49).

RESULTS

Era depletion causes accumulation of 30S subunit assembly intermediates

We created a strain that allowed for the controlled expression of Era under an arabinose inducible promoter and we used it to determine how Era depletion impacts the distribution of ribosomal particles and their protein composition in *E. coli* cells. This strain exhibited a growth phenotype consistent with previously characterized Era-depleted strains (Supplementary results and Supplementary Figure S1). Crude ribosomes were extracted from cells grown under permissive (+arabinose) and restrictive (-arabinose) conditions, layered onto a 10–30% (w/v) sucrose gradient and subjected to ultracentrifugation. In wild-type *E. coli* cells, between 2 and 5% of the 30S subunits are immature and remain typically dissociated instead of forming 70S ribosomes (17,28). Consistent with that data, 3% of the 30S subunits were immature and dissociated from 50S subunits when the strain was grown under permissive conditions. However, growth in restrictive conditions increased the percentage of free immature 30S subunits to 67%, significantly decreasing the proportion of 70S ribosomes (Figure 1A; top panel). This percentage was significantly higher than what has been reported in the past for other non-essential assembly factor knock-out strains (Δ*rimM*, Δ*yjeQ*, Δ*rbfA*) (17,28,55,56) consistent with a more substantial defect in the 30S subunit assembly process.

Next, we used quantitative mass spectrometry (qMS) to determine the r-protein composition of the 30S particles purified from either parental or Era-depleted strains. Based on their occupancy levels in the $30S_{Era\text{-}depleted}$ particles, r-proteins were divided into three groups (Figure 1B and Supplementary Figure S2). Group 1 included most r-proteins, which were present stoichiometrically in all 30S particles, suggesting that their binding was independent of Era. Conversely, group 3 proteins, bS1 and bS21, were completely missing from $30S_{Era\text{-}depleted}$ particles revealing that their binding was severely affected by Era depletion. Finally, group 2 proteins, uS2, uS3 and uS5, showed intermediate occupancy levels in $30S_{Era\text{-}depleted}$ particles, suggesting a partial Era-dependence for their binding. We noted that occupancy of bS20 was sub-stoichiometric in small subunit particles derived from either Era-depleted cells or parental cells, consistent with protein dissociation during purification of the subunits.

Painting the Nomura map (57–59) according to these r-protein groups (Figure 1C) revealed that the protein complement of the $30S_{Era\text{-}depleted}$ particles is consistent with the binding hierarchy defined by the assembly map. Inspection of mature 30S subunit crystal structure (60) and

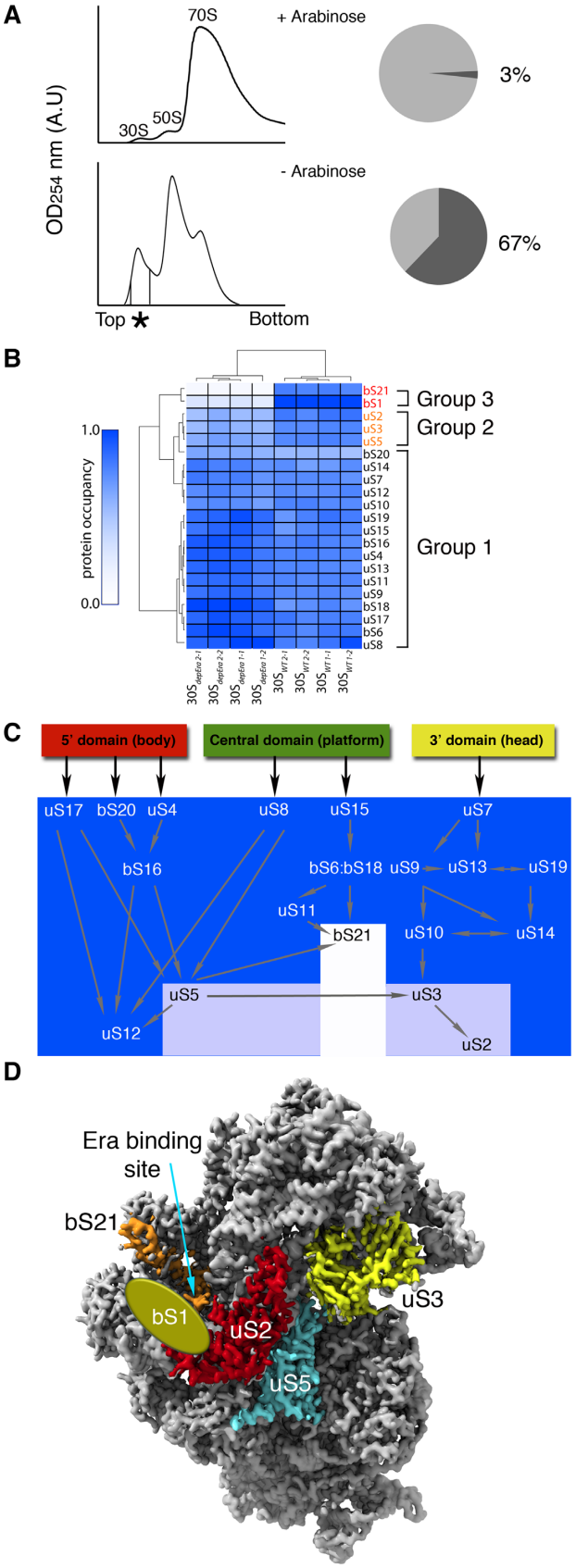

Figure 1. Ribosomal proteins and assembly factors content of the 30S particles in Era depleted cells. (**A**) Ribosomal profiles of the Era depleted strain under Era expression (+arabinose) and Era depletion (-arabinose) conditions. The asterisk and vertical lines in the bottom gradient indicate the fractions that provided the purified $30S_{Era\text{-}depleted}$ particles for the qMS and cryo-EM experiments. The pie charts indicate the fraction of ribosomal particles represented by free 30S subunits. (**B**) Heat map showing protein abundance of the 30S particles purified from the parental strain and the Era depleted strain grown under (-arabinose) conditions. Protein abundance is shown relative to a purified 70S particle. Occupancy patterns were hierarchically clustered revealing three groups, which are marked. Proteins in each group are labeled in a different color. Sample replicas were also hierarchically classified and clustered in two groups indicated as $30S_{depEra}$ ($30S_{Era\text{-}depleted}$ particles purified from Era depleted strain grown under (-arabinose) conditions) and $30S_{WT}$ (30S subunits purified from parental strain). (**C**) Protein occupancy levels from the qMS analysis of the $30S_{Era\text{-}depleted}$ particles were plotted in the Nomura assembly map of the 30S subunit using the same color coding as in panel (A). (**D**) The r-proteins found to be sub-stoichiometric by qMS are shown in a color different from gray in the structure of the mature 30S subunit. The entire r-protein bS1 is not shown for clarity. The oval shape labeled as bS1 indicates the binding site of the N-terminal region of this protein to the 30S subunit. Ribosomal proteins found on full occupancy in the $30S_{Era\text{-}depleted}$ particles are shown in gray.

cross-linking mass spectrometry data localizing bS1 binding site (61) showed that sub-stoichiometrically bound proteins (group 2 and 3) associate near the Era-binding site on the platform region of the particle (18) (Figure 1D). The conspicuous co-localization of these r-proteins suggested that Era may be assisting the entry of these proteins.

Taken together this analysis showed that a large proportion of the particles isolated form Era-depleted cells were immature and in the late stages of the assembly process.

The immature 30S particles accumulating in the Era-depleted strain range from early to late assembly intermediates

To further understand the role of Era in the assembly of the 30S subunit, we determined an ensemble of structures present in the $30S_{Era\text{-}depleted}$ particles using high-throughput, single particle cryo-EM. Our dataset included over 800 000 particle images of purified $30S_{Era\text{-}depleted}$ particles and, after subjecting this dataset to multiple rounds of 3D image classification and initial map determination, we obtained a collection of 16 cryo-EM maps (Figure 2).

These 16 cryo-EM maps provide a direct visualization of the 30S subunit as it assembled (Supplementary Movie S1). Classes A, B and C represented particles at very early stages of assembly. These particles exhibited density corresponding to the body of the 30S subunit and lacked platform or head domains. Notably, in these maps the body had not fully matured as rRNA helices and could not be readily assigned. Class D contained particles appearing to undergo maturation of the body and platform, but without starting to significantly fold the head. Classes E–H appeared to be folding the three domains simultaneously. The remaining classes (I–P) resembled successively more mature assembly intermediates with body, platform and head domains progressively closer in structure to the mature subunit. No class corresponding to fully mature 30S subunit was observed.

Our structures of isolated body domains (classes A–C), which are composed of the 5′ and central domains are largely in agreement with previous work establishing that

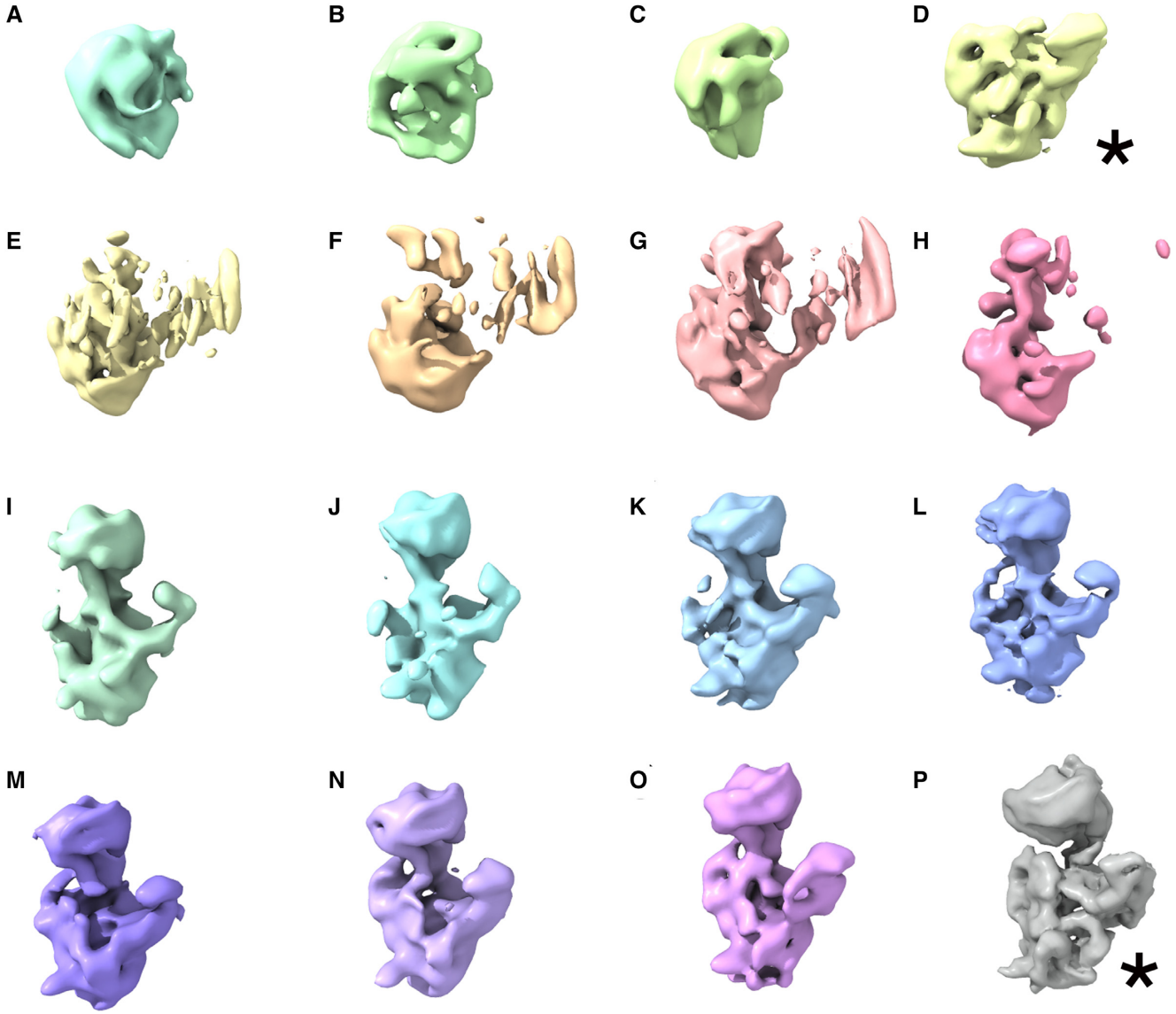

Figure 2. Immature 30S particles accumulating in the Era-depleted strain. (**A**–**P**) Cryo-EM maps obtained from a sample containing purified $30S_{Era\text{-}depleted}$ particles using 3D image classification approaches. The most abundant classes are marked by an asterisk. Classes D and P represented the 22% and 50% of the population, respectively. The remaining classes accumulated only a 28% of the particle population.

rRNA folding occurs 5′ to 3′ (2,62). Notably, however, our observation that the body, platform and head domains in classes E–P are partially unfolded indicates that, at least in the absence of Era, rRNA folding is not necessarily sequential and that maturation of all three major domains of the 16S rRNA can occur in concert.

Particles assigned to classes D and P represented the 22% and 50% of the population, respectively and it was possible to obtain high-resolution structures for these assembly intermediates (see section below). All the other remaining classes accumulated only 28% of the particle population and consequently only rendered maps at modest resolution (10–15 Å). However, they still provided sufficient detail to visualize the overall folding of the 16S rRNA domains (Figure 2 and Supplementary Movie S1).

Folding of the platform domain of the 30S subunit requires Era

The map for class D refined to 4.8 Å resolution (Figure 3A and Supplementary Figure S3A). Local resolution analysis showed that the body of the particle is the most defined region, whereas the platform is less well resolved, likely due to intrinsic flexibility caused by the maturation events still ongoing in this domain (Supplementary Figure S3B). As we were unable to build an atomic model at this resolution, we docked the X-ray structure of a complete 30S subunit (60) into this map to visualize how structural elements in class D deviated from the mature structure. This analysis revealed that the density corresponding to the head domain was completely missing in the cryo-EM map of the assembly intermediate, whereas density for the rRNA in the body and platform was present. Notably, the body and platform den-

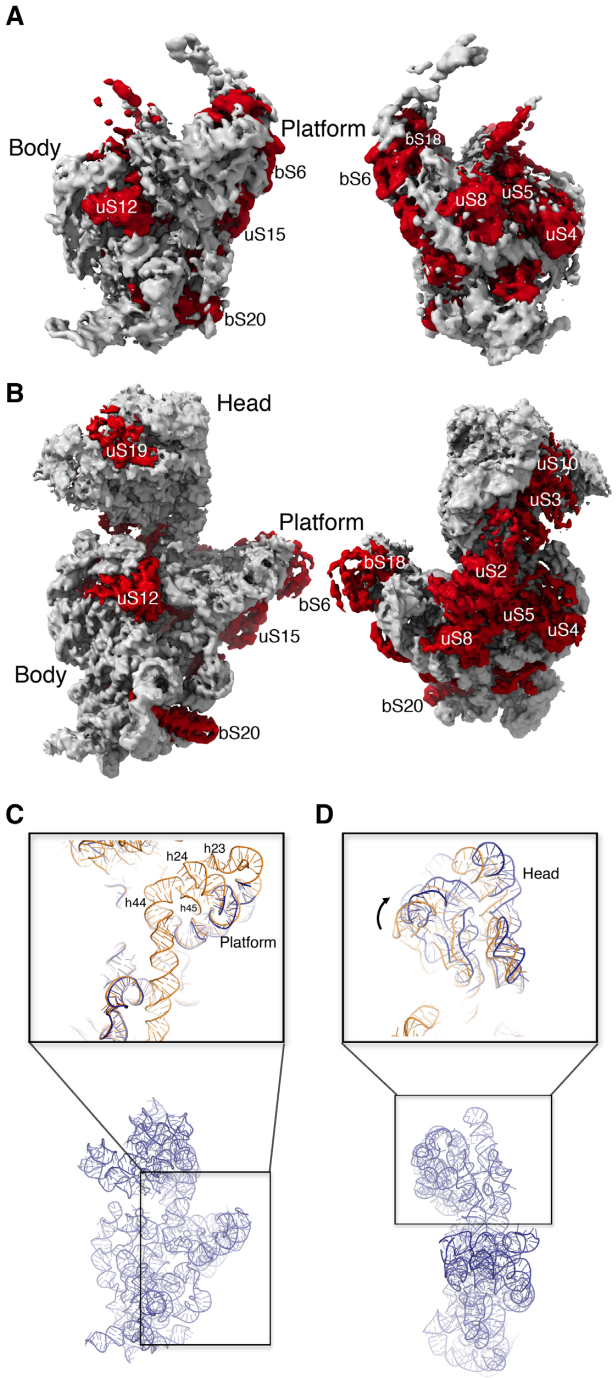

Figure 3. Cryo-EM structures of the most abundant $30S_{Era\text{-}depleted}$ particles. (**A**) Front and back view of the cryo-EM map of the $30S_{Era\text{-}depleted}$ particle class D. Ribosomal proteins and rRNA in the structure are colored in red and light gray, respectively. (**B**) Similar representation of the cryo-EM map of the $30S_{Era\text{-}depleted}$ particle class P. (**C**) Zoom-in-view of the 3′ minor and central domains of the atomic model obtained for the $30S_{Era\text{-}depleted}$ particle class P. The area framed with a black square in the overall view of the atomic model (r-proteins removed for clarity) at the bottom is shown enlarged in the top panel. The top panel shows the superimposition of the atomic model for the mature 30S subunit (orange) (PDB ID: 4V4Q) and the corresponding region on the model obtained for the $30S_{Era\text{-}depleted}$ particle (dark blue). (**D**) Zoom-in-view of the 3′ major domain of the atomic model obtained for the $30S_{Era\text{-}depleted}$ particle class P. This region of the model is compared in the top panel with the atomic model of the mature 30S subunit following the same color code as in panel (C). Ribosomal proteins have been removed for clarity.

sity observed to be deviated substantially from the tracing of the atomic model of the mature 30S subunit indicating that these regions are still in an immature conformation. The cryo-EM map was also missing density for all the r-proteins in the head, as well as uS2 and uS5 in the body and bS21 in the platform.

The cryo-EM map for class P, the most mature of the assembly intermediates, refined to 3.8 Å resolution (Figure 3B and Supplementary Figure S3A) with the highest local resolution in the body region of the map. Peripheral domains including the front of the head and platform regions exhibited lower local resolution, again consistent with an intermediate still undergoing maturation. The resolution of this cryo-EM map was sufficient to produce an atomic model from the cryo-EM map (Supplementary Figure S4 and Supplementary Table S1), which we used to compare this assembly intermediate to the mature 30S subunit (Figure 3C and Supplementary Movie S2). The platform and 3′ minor domain exhibited the most striking structural differences. Indeed, in the platform, density for helices 23 and 24 was absent or highly fragmented, and helices 44 and 45 (nucleotides 1397–1534) of the 3′ minor domain were completely invisible (Supplementary Movie S2). We interpret these fragmented regions of the map as indications that these elements have not fully matured. Finally, all structural elements were present in the head domain, but this entire rigid body was tilted away from the platform (Figure 3D). The remainder of the structure was largely indistinguishable from the mature subunit and exhibited complete density for r-proteins in all four domains except for uS7, uS9, uS13 and uS19 in the head, and uS11 and bS21 in the platform, which each showed a highly fragmented density or lacked density completely (Figure 3B and Supplementary Movie S2). Combining this structure with our qMS data (Figure 1B), we concluded that proteins bS21 and bS1 are completely absent whereas proteins uS7, uS9, uS11, uS13 and uS19 are likely bound in a flexible manner not easily resolved by cryo-EM.

The structural differences of class P with the mature subunit suggest that during the folding of the platform domain, helices 23 and 24 failed to adopt the mature conformation in the absence of Era. However, the assembling particles were able to skip the folding of this motif and re-route their assembly pathway to continue with the maturation of the head domain, which is downstream of helices 23 and 24 (63–66). Therefore, we concluded that the folding of helices 23 and 24 represents a critical folding barrier during 30S subunit maturation and Era mediates efficient folding of these helices.

Era expression promotes maturation of helices 23 and 24 in the 30S subunit platform domain

We next used dimethyl sulfate (DMS) footprinting to inspect the structure of the 16S rRNA platform domain with single nucleotide resolution in various Era-limited cells. Specifically, cells were collected before Era depletion (Era pre), after Era depletion (Era depleted) and at various times after Era re-expression (Era+) and were treated with DMS for 0.5, 1 or 2 min (Figure 4A), and the methylation pattern in the 16S central domain was detected by primer extension

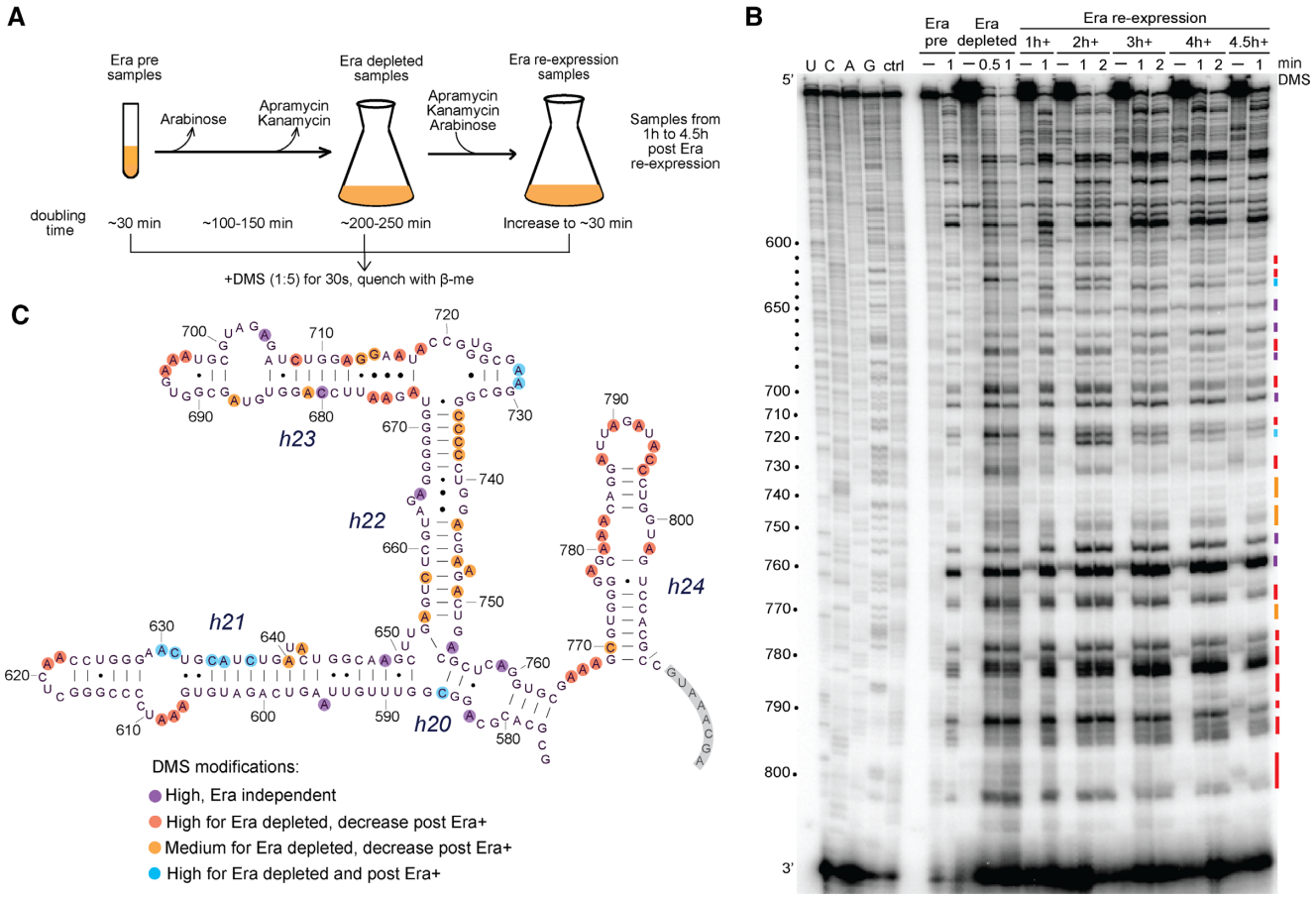

Figure 4. *In vivo* DMS footprinting of Era-dependent changes in the 16S central domain. (**A**) Scheme of the *in vivo* DMS footprinting experiment after Era depletion and re-expression. (**B**) DMS modification patterns of different Era samples as detected by extension of primer 812 (Supplementary Table S4). The Era pre, Era depleted and Era re-expression cells were untreated (–) or modified with DMS for 0.5, 1 or 2 min. DMS modified nucleotides are highlighted with colored bars (right). The nucleotide numbers are indicated to the left of the sequencing ladder, and the unextended primer is marked (3′). (**C**) DMS-modified nucleotides on the 16S rRNA secondary structure are colored based on the effect of Era as indicated in the key and illustrated in Supplementary Figure S5. The primer binding location is shaded gray.

(Figure 4B and Supplementary Figure S5). We mapped the 5′ end of the rRNA by primer extension to confirm that the ratio of immature 17S to mature 16S RNA increased upon Era depletion and decreased when Era expression was restored (Supplementary Figure S6).

We found that helices 23 and 24 in the central domain were highly modified by DMS in Era depleted samples, compared to cells probed before Era depletion (Era pre) or after Era was re-induced (Era+) (red and orange in Figure 4B and C). This result is consistent with the cryo-EM maps obtained for the $30S_{Era\text{-}depleted}$ particles purified from cells grown under Era depletion conditions. All of these structures exhibited non-mature conformations of the platform domain and had missing or broken densities for helices 23 and h24. In sum, these results confirm that these two helices were not natively folded in the absence of Era. Likewise, nucleotides in helix 22 also showed increased DMS modification upon Era depletion and enhanced protection when Era was restored, suggesting that Era directly or indirectly stabilizes the structure of helix 22 (orange in Figure 4B and C). As density for helix 22 is observed in the class P cryo-EM maps, this chemical probing result implies that helix 22 is likely immature in most of the other classes (classes A–O), which constitute ∼50% of all Era-depleted particles (Figure 2). We also observed delayed changes to the DMS modification pattern of helix 21, in which an internal bulge in helix 21 folds only 1 h after Era re-expression (blue in Figure 4C and Supplementary Figure S5C). The base of helix 21 is recognized by ribosomal protein uS8, but its tip extends away from the central domain to contact the solvent side of the 30S subunit 5′ domain. This timing suggests that Era enables structural changes at the interface of the 5′ and 3′ domains during 30S assembly, in agreement with previous *in vitro* footprinting results that revealed conformational changes in the region around r-protein uS8 and slow folding of h21 during 30S assembly (67). Taken together, our in-cell DMS probing results are consistent with the observed cryo-EM structures and highlight Era's role in assembly of the 30S subunit platform.

Era binding to the mature 30S subunit destabilizes helix 44 and decoding center

Cells often employ quality control mechanisms to survey nascent and mature ribosomes and ensure their function-

ality (68–70). Recently, it was suggested that in addition to its function as an assembly factor, YjeQ may also test the proofreading ability of the 30S subunit (22). Thus, to investigate a potential role for Era in ribosome quality control, we assayed Era's ability to interact with mature ribosomes, and determined the effect of this interaction in the 30S subunit using cryo-EM.

We first tested the ability of Era to interact with the mature 30S subunit using a dissociation experiment (71). This assay exploits the ability of Era to split 70S ribosomes into 50S and 30S subunits (18). Era was mixed and incubated with purified 70S ribosomes in buffer containing either GDP, GTP, GMPPNP or no nucleotide. Subsequently, ribosomal particles were separated by sucrose density ultracentrifugation (Figure 5A). We found that most of the ribosomes remained as 70S particles after mixing a 5-fold excess of Era in the absence of nucleotide. However, we observed significant 70S dissociation when Era was added in the presence of buffer containing one of the nucleotides. Effective splitting was both nucleotide- and Era-dependent as incubation of 70S particles with GMPPNP alone had no effect.

Taking these results into consideration, we mixed mature 30S subunits with Era in a buffer containing GMPPNP and collected cryo-EM images that were subjected to single particle analysis and classification routines. The 3D classification analysis identified two main classes of particles. The first group (class I) produced a map that refined to 5.4 Å resolution (Supplementary Figure S7) and represented 12% of the particle population. It had densities representing all rRNA helices and r-proteins present in the mature 30S subunit, including helix 44. Therefore, we concluded that the map for class I represented mature 30S subunits that did not enter in contact with Era.

The second class of particles (class II) produced a map that refined to 3.9 Å resolution (Supplementary Figure S8A). Local resolution analysis showed that the highest resolution values were observed in the body domain of the subunit. Peripheral domains including the front of the head and platform regions exhibited lower resolution suggesting higher flexibility in these domains (Supplementary Figure S8B). The cryo-EM map (Figure 5B and C; Supplementary Movie S3) presented significant differences in the 3′ minor domain with the mature 30S subunit, which we interpreted as Era-induced conformational changes. For example, density for helix 44 was completely invisible, and density at the tips of helices 23 and 24 was mildly fragmented (Figure 5B). Density was also lacking for bS1, uS7, bS21 and the N-terminal region of uS13 (Figure 5B and C). All other regions of the structure resembled the mature 30S subunit. Surprisingly, we could only observe a small and fragmented density near uS2 in the cleft region between platform and head that could be assigned to Era, suggesting that that unlike *T. thermophilus* Era (18), *E. coli* Era binds to this region either transiently or in a flexible manner (Figure 5C). In conclusion, the obtained cryo-EM map for class II suggested that Era has the ability to destabilize functionally essential regions of the mature 30S subunit, including the key elements of the decoding center such as helix 44.

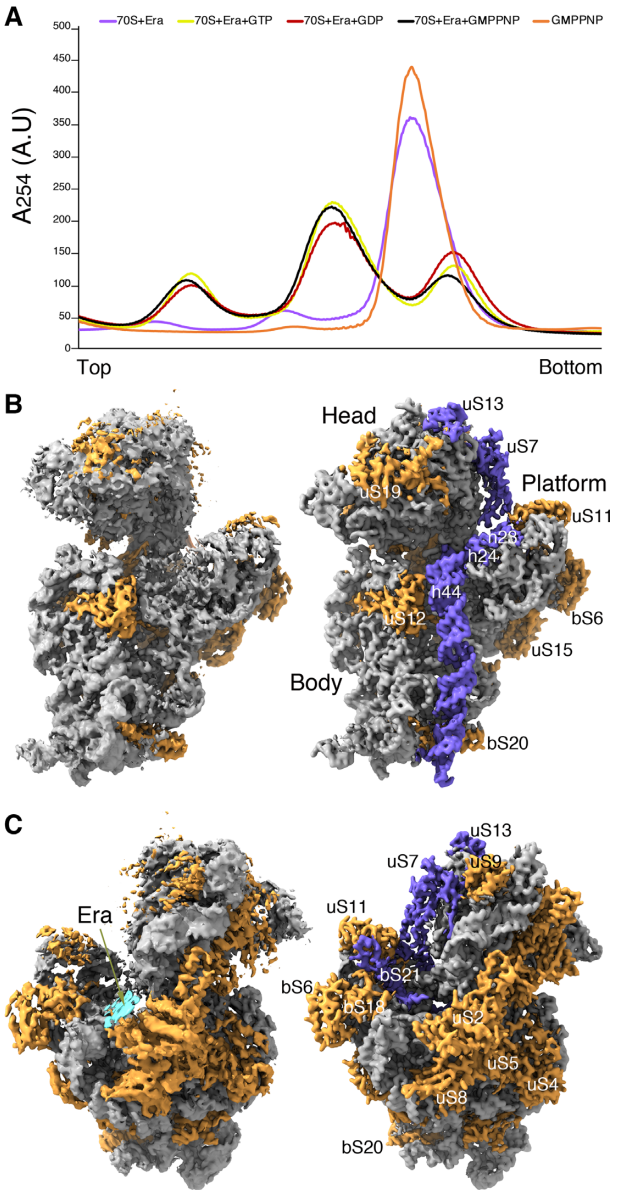

Figure 5. Era dissociates 70S ribosomes and destabilizes helix 44 and decoding center. (**A**) Ribosome profiles obtained during the 70S dissociation experiments. Plot lines from the reaction containing GMPPNP, GTP, GDP or no nucleotide are shown. All reactions contained a 5-fold excess of Era with respect to the 70S ribosomes. (**B**) Comparison of the cryo-EM map obtained for the Era-treated 30S (class II) (left panel) with the structure of the mature 30S subunit (PDB ID: 4V4Q) (right panel). The r-RNA and r-proteins are labeled and colored in grey and orange, respectively in both structures. Structural elements absent in the cryo-EM map obtained for the 30S particles treated with Era are colored in blue in the structure of the mature 30S subunit. This panel shows a front view of the structures. (**C**) Comparison of the back view of the cryo-EM map obtained for the Era treated 30S particles (class II) (left panel) with the structure of the mature 30S subunit (right panel) using the same coloring scheme as in panel (**B**). For clarity, bS1 is not shown in the mature 30S subunit. The fragmented density potentially representing Era is indicated with an arrow and colored in cyan.

Era destabilization of helix 44 blocks binding of YjeQ to the 30S subunit

Previously, Cambell and Brown showed that overexpression of Era suppresses the slow growth phenotype of *ΔyjeQ* cells suggesting a functional interplay between the factors (19). Thus, we investigated whether these factors could simultaneously bind the mature 30S, and whether the presence of YjeQ could stabilize Era binding. First, we used microscale thermophoresis (MST) to measure whether pre-binding of Era to the 30S subunit affected the binding of YjeQ to the 30S. Consistent with previous studies (17), YjeQ exhibited high binding affinity to the 30S subunit with a K_d value of 58.5 ± 47 nM. However, mixing a 10- or a 20-fold molar excess of Era with the 30S subunits prior to addition of YjeQ, increased the K_d of the interaction between YjeQ and mature 30S subunits to 1.1 ± 0.6 and 2.3 ± 1.2 μM, respectively. Similarly, pre-binding of YjeQ to the 30S subunit also decreased the binding affinity of Era 5-fold (Supplementary Figure S9). These results indicated that binding of Era or YjeQ to the 30S subunit dramatically decreased the affinity of the other factor to the subunit.

To determine the structural bases explaining the decreased affinity of one factor upon pre-binding of the other, we set up an assembly reaction containing mature 30S subunits plus a molar excess of YjeQ and Era. Using cryo-EM and 3D classification approaches, we found two populations of particles coexisting in the assembly reaction. Class I included 36% of the particles and the obtained map for this class refined to 4 Å resolution (Supplementary Figure S7). Similarly to the reaction containing Era protein and 30S subunits only, the class I map derived from this reaction also represented mature 30S subunits. It exhibited densities for all the structural motifs present in the mature 30S subunit and a well-defined density for helix 44.

The map for class II refined to 3.5 Å resolution (Supplementary Figure S10A). The highest resolution values were observed in the body domain, whereas the front of the head and platform regions exhibited higher flexibility and produced a map with lower resolution values (Supplementary Figure S10B). Previously published structures showed that YjeQ binds to the decoding center and stabilizes helix 44 (22,71–73). However, we found no additional density in this area of the map that could be assigned to YjeQ and helix 44 was also completely unfolded (Figure 6B). Like the class II map obtained from the reaction containing mature 30S subunits and Era protein only, this cryo-EM map lacked density for uS7 and the N-terminal region of uS13 (Figure 6B and Supplementary Movie S4). However, we found two main differences as well with this map. First, the 30S particles treated with Era and YjeQ showed a defined density for r-protein bS21 (Figure 6C) and second, it also presented a highly fragmented density in the cleft region between the head and platform. This region is thought to be the Era-binding site in the mature 30S subunit (18). Masked classification on the Era-binding region with subtraction of the signal from the rest of the complex did not define this density with sufficient details to unambiguously assign it to Era (Figure 6C) and indicated the flexible or transient nature of Era binding to these ribosomal particles. This cryo-EM map suggested that one of the mechanisms by which Era decreases the affinity of YjeQ for the mature 30S subunit is by inducing the undocking of helix 44.

DISCUSSION

Role of Era in 30S subunit assembly

Prior structural and biochemical analysis of the immature 30S particles that accumulate in Δ*yjeQ* (74), Δ*rimM* (28,56), Δ*rimP* (63) and Δ*yjeQ*Δ*rbfA* (75) strains have proven powerful in identifying the role of these non-essential assembly factors. Similar approaches have been applied to study the assembly process of the 50S subunit by genetically removing either assembly factors (76) or essential r-proteins (30). Here, we have extended this methodology to the essential 30S subunit assembly factor Era and employed high-throughput cryo-EM data collection to achieve higher resolution that was possible in prior studies of the 30S.

Previous negative staining EM visualization of 30S particles isolated from wild-type *E. coli* and a Δ*rimP* strains (63) and from *in vitro* reconstitution reactions (64) revealed that assembly of the 30S subunit is sequential (from 5′ to 3′) and that folding of the head domain only occurs upon completion of the folding of the 5′ and central domain. In striking difference, our cryo-EM analysis suggests that in the assembly of the 30S subunit, at least in the absence of Era, all three major domains of the 16S rRNA can co-mature. In particular, classes E–H identified within the $30S_{Era\text{-}depleted}$ particle population (Figure 2) appeared to be clearly folding the three domains simultaneously.

Our structures also revealed that most 16S rRNA elements were able to fold even when Era was depleted. Notably, we found that helices 23 and 24 in the platform domain failed to mature upon Era depletion. Given their proximity to the putative Era-binding site, we posit that Era is directly involved in the maturation of helices 23 and 24. As described above, helices 23 and 24 are thought to mature early in the assembly process when Era is present (63–66) and, if ribosome assembly is strictly sequential, one would have expected assembly to stall at this point and the accumulated intermediates to be very immature (Figure 7). Instead, we observe a significant number of late assembly intermediates (classes G–P), implying that particles re-routed their folding pathway to continue the maturation of their other structural motifs (Figure 7) while waiting for maturation of Era-dependent elements.

The large percentage (22%) of particles adopting the conformation described by class D probably represent the assembly intermediates unsuccessfully attempting to properly fold these helices, but before finding an alternative assembly pathway to continue their maturation and producing the subsequent classes (classes F–P). This interpretation aligns well with previous studies establishing that assembly of the 30S subunit occurs through multiple parallel assembly pathways (1,2) and recent work illustrating dynamic re-routing of assembly flux through parallel pathways in the large subunit (30).

Interestingly, helices 44 and 45 are also immature in each of our structures suggesting that their maturation either directly depends on Era or, instead, requires proper maturation of helices 23 and 24 in the platform domain. We fa-

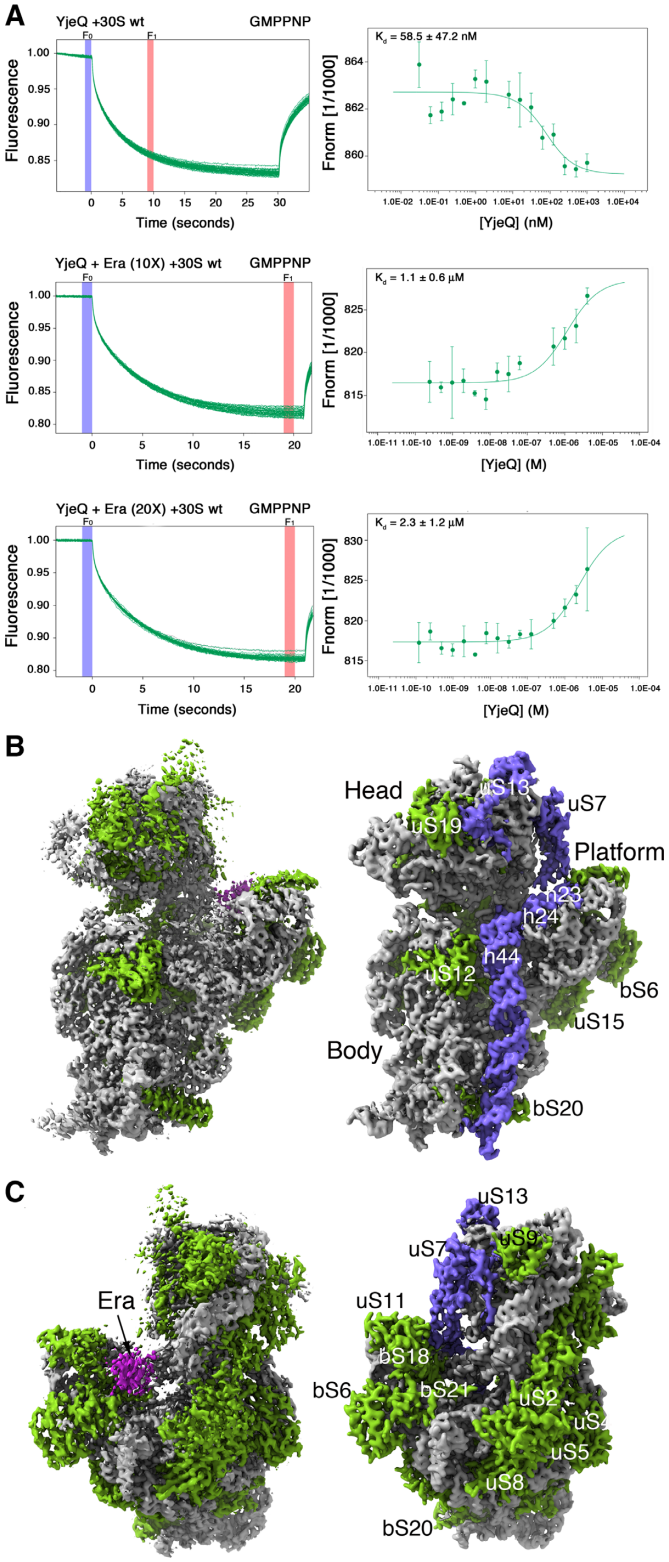

Figure 6. Era blocks binding of YjeQ to the 30S subunit. (**A**) Analysis of the interaction of YjeQ with the mature 30S subunit by MST. Ribosomal particles were fluorescently labeled and maintained at constant concentration in the three assays. In one assay, the ribosomal subunits were present by themselves and unlabeled YjeQ was titrated into the reaction (top panels). In the other two assays, before YjeQ was added at increasing concentrations, the mature 30S subunits were first mixed with a 10-fold (middle panels) or 20-fold excess of Era (bottom panels). After a short incubation with YjeQ, reactions were loaded into the capillaries and the MST signal of the labeled ribosomal particles (left panels) was measured. Measured changes in the MST response were used to produce curves that plotted the F_{norm} (%) = F_1/F_0 versus the logarithm of YjeQ concentration. The F_1 and F_0 regions of the fluorescence time traces used to calculate F_{norm} (%) are indicated in the panel (A). (**B**) Front and (**C**) back views of the cryo-EM map obtained for the Era+YjeQ-treated 30S (class II) (left panels). Ribosomal proteins and rRNA in the structure are colored in green and light gray, respectively. Equivalent views of the mature 30S subunit are shown in the right panels with the structural components displayed using the same color scheme. Structural elements absent in the cryo-EM map obtained for the 30S particles treated with Era and YjeQ are colored in blue in the structure of the mature 30S subunit. For clarity, bS1 is not shown in the mature 30S subunit.

vor the later model as folding of helices 44 and 45 including the decoding center are thought to be final maturation steps before the 30S subunit becomes functionally active and the factors YjeQ and RbfA have previously been implicated in facilitating this step (22,71,74,77).

Role of Era in ribosome homeostasis

Prior structural work (13,18) has also suggested that Era might block premature translation initiation by 'immature' small subunit particles. Suggested models include: (i) blocking access to the anti-Shine-Dalgarno (SD) sequence near the 3′ end of the 16S rRNA; and (ii) preventing the binding of bS1, a r-protein necessary for the SD / anti-SD interaction to the 30S subunit. The 70S dissociation experiments performed herein indicate that Era may also prevent translation initiation by *mature* 30S subunits. Our subsequent structural analysis of the mature 30S particles treated with Era revealed a complete unfolding of helix 44 and reversion of the decoding center to an immature state. As helix 44 contains the b2a inter-subunit bridge that is essential for subunit joining, this Era-treated particle would not be competent for translation.

Reversion of ribosomal structural motifs to an immature state is not unprecedented. Indeed, earlier studies have described this phenomenon upon removal of r-proteins (31) or binding of the assembly factor YjeQ (71). Our analysis demonstrates that Era shares this ability and opens the possibility that cells may utilize these assembly factors to revert mature, active ribosomes into inactive, immature particles.

The physiological conditions in which this function of Era or other assembly factors sharing this ability becomes relevant for survival or fitness are still unclear. Possibilities include the participation of Era on active dissociation of hibernating RMF (ribosome modulation factor,) HFP (hibernation promoting factor)-100S and RaiA (ribosome-associated inhibitor A)-70S ribosomes that *E. coli* assembles during stationary phase to stop protein synthesis and reduce energy consumption (78). A recent publication has provided the first insight into GTP-dependent dissociation mechanisms of 100S ribosomes by the widely conserved GTPase HflX (79). However, deletion of hflX had only a moderate effect on the fraction of dimerized ribosomes, suggesting that HflX is not solely responsible for dissociation and that other protein factors such as Era could also be involved in the reactivation mechanisms. It is also

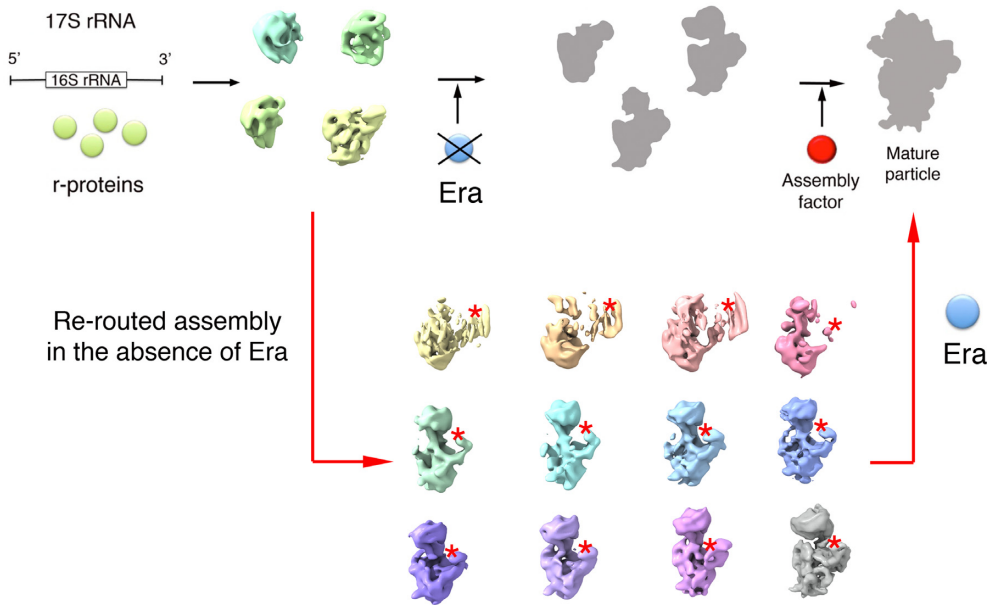

Figure 7. Era depletion causes re-routing of the assembling 30S particles. Diagram summarizing the effect of Era depletion on the assembly of 30S subunits. Cellular depletion of the essential assembly factor Era does not stall the assembly of the 30S subunit, causing accumulation of assembly intermediates upstream of the reaction catalyzed by Era. Rather, in the absence of the Era, the 30S particles are unable to fold helices 23 and 24 in the platform domain; however, they re-route their folding pathway and continue the maturation of other structural motifs. During this process, all of the 16S rRNA domains of the 30S subunit fold independently and simultaneously accumulating a variety of assembly intermediates that were characterized in this study using cryo-EM. The red asterisks indicate that helices 23 and 24 still adopt an immature conformation in all of these structures. Only re-introduction of Era in the cells allow these assembly intermediate to reach a mature state. The ribosomal particles shown as gray flat profiles indicate the physiological assembly intermediates that exist in the cell when Era is present at normal concentrations. These particles are capable of folding helices 23 and 24 normally and reach the mature state.

plausible the cell uses Era and other destabilizing assembly factors to initiate ribosome degradation during starvation. Conditions that increase the formation of ribosomal subunits lead to enhanced degradation, while conditions favoring the presence of intact 70S ribosomes prevent or reduce breakdown (80). Understanding the physiological conditions triggering these potential new functions of Era in ribosome homeostasis remains to be investigated.

Functional interplay between Era and YjeQ

Prior genetic experiments suggested functional interactions between Era and other assembly factors. For example, overexpression of Era suppressed the ribosome assembly defects in a Δ*rbfA* strain (10), and overexpression of KsgA, which methylates residues in h45, suppressed the cold-sensitive phenotype of Era E200K (81). Although these factors are thought to bind at non-overlapping sites on the 30S subunit, (18,82), these results suggested that Era could facilitate the function of RbfA or KsgA and potentially substitute for them.

The present study investigates the functional interplay between Era and YjeQ and extends the work of Campbell and Brown (19), who reported that Era overexpression increases polysome count and ameliorates the growth defect of a *yjeQ* null strain. YjeQ is thought to act during 30S subunit assembly by aiding in folding of helix 44 and decoding center (22,71–74). Our work suggests that Era has the opposite effect on mature ribosomes, as it appears to promote unfolding of helix 44 during the Era-dependent subunit splitting reaction (Figure 6). This result implies that Era binds to the immature 30S subunit independently from YjeQ. However, it remains unclear from these data how Era overexpression compensates for YjeQ function.

Role of Era in processing and folding of the rRNA

Given that Era recognizes the $_{1531}$AUCACCUCC$_{1539}$ sequence, which is close to the mature 3′ end of 16S rRNA (13,15), Era has also been implicated in rRNA processing regulation. In these models, it is suggested that Era binding to this sequence could induce a conformational change in the 17S rRNA that promotes auto-cleavage or exposes the 3′ end of the 17S rRNA to RNases (10). Alternatively, crystallography studies (13,15) propose that Era binding actually protects the rRNA from premature cleavage by RNAses during the ribosome assembly process. Our finding that Era depleted cells have higher ratios of 17S rRNA molecules containing the 5′ precursor sequence but not the 3′ sequence (Supplementary Results) is consistent with Era playing a protective role by ensuring that the processing of the 3′ end does not occur prematurely. This putative protective role is also consistent with a recent model (83) proposing that the endoribonuclease YbeY forms a complex with Era to guide accurate RNAse-mediated cleavage of the terminal 33 nucleotides at the 3′ end of the 17S rRNA.

Overall, this study found that folding of helices 23 and 24 in the platform region of the 30S subunit directly or indirectly relies on Era. In the absence of this factor, particles skipped the folding of these two helices and were re-

routed in their folding pathway. The assembling particles did not follow a sequential (from 5′ to 3′) folding and all three major domains of the 16S rRNA co-matured. In addition, we found that treatment of mature 30S subunits with Era destabilizes functionally essential regions of the 30S subunit. Further investigations in this newly discovered capacity of Era will unravel the putative role of this essential protein factor in mechanisms of ribosome homeostasis, including the reactivation of hibernating ribosomes or the triggering of ribosome degradation.

DATA AVAILABILITY

The EMDB IDs assigned to the structures presented here are: $30S_{Era\text{-}depleted}$ class D (0481), $30S_{Era\text{-}depleted}$ class P (0482), Era-treated 30S class II (0483) and Era+YjeQ-treated 30S class II (0484). The coordinates for the atomic model built for the $30S_{Era\text{-}depleted}$ class P have been deposited in the Protein Data Bank with accession code (6NQB).

SUPPLEMENTARY DATA

Supplementary Data are available at NAR Online.

ACKNOWLEDGEMENTS

We are grateful to Dr Eric Brown and Dr Jean Philippe Cote for their technical assistance in the production of the Era depleted *E. coli* strain. We thank Dr Kelly Sears, Dr Mike Strauss and other staff members of the Facility for Electron Microscopy Research (FEMR) at McGill University for help in microscope operation and data collection. We acknowledge Jingyu Sun for providing purified Era for MST experiments and Clara Ortega for assistance with graphic design. Titan Krios cryo-EM data were collected at FEMR (McGill). FEMR is supported by the Canadian Foundation for Innovation, Quebec government and McGill University.

FUNDING

Canadian Institutes of Health Research [PJT-153044 to J.O.]; NIH grant from NIGMS [R01GM110248 to R.A.B.]; NIH grant from NIA [5R00AG050749 to J.H.D.]. Funding for open charge: Canadian Institutes of Heath Research.
Conflict of interest statement. None declared.

REFERENCES

1. Adilakshmi,T., Ramaswamy,P. and Woodson,S.A. (2005) Protein-independent folding pathway of the 16S rRNA 5′ domain. *J. Mol. Biol.*, **351**, 508–519.
2. Talkington,M.W., Siuzdak,G. and Williamson,J.R. (2005) An assembly landscape for the 30S ribosomal subunit. *Nature*, **438**, 628–632.
3. Shajani,Z., Sykes,M.T. and Williamson,J.R. (2011) Assembly of bacterial ribosomes. *Annu. Rev. Biochem.*, **80**, 501–526.
4. Leipe,D.D., Wolf,Y.I., Koonin,E.V. and Aravind,L. (2002) Classification and evolution of P-loop GTPases and related ATPases. *J. Mol. Biol.*, **317**, 41–72.
5. Takiff,H.E., Chen,S.M. and Court,D.L. (1989) Genetic analysis of the rnc operon of Escherichia coli. *J. Bacteriol.*, **171**, 2581–2590.
6. March,P.E., Lerner,C.G., Ahnn,J., Cui,X. and Inouye,M. (1988) The Escherichia coli Ras-like protein (Era) has GTPase activity and is essential for cell growth. *Oncogene*, **2**, 539–544.
7. Anderson,P.E., Matsunaga,J., Simons,E.L. and Simons,R.W. (1996) Structure and regulation of the Salmonella typhimurium rnc-era-recO operon. *Biochimie.*, **78**, 1025–1034.
8. Sato,T., Wu,J. and Kuramitsu,H. (1998) The sgp gene modulates stress responses of Streptococcus mutans: utilization of an antisense RNA strategy to investigate essential gene functions. *FEMS Microbiol. Lett.*, **159**, 241–245.
9. Minkovsky,N., Zarimani,A., Chary,V.K., Johnstone,B.H., Powell,B.S., Torrance,P.D., Court,D.L., Simons,R.W. and Piggot,P.J. (2002) Bex, the Bacillus subtilis homolog of the essential Escherichia coli GTPase Era, is required for normal cell division and spore formation. *J. Bacteriol.*, **184**, 6389–6394.
10. Inoue,K., Alsina,J., Chen,J. and Inouye,M. (2003) Suppression of defective ribosome assembly in a rbfA deletion mutant by overexpression of Era, an essential GTPase in Escherichia coli. *Mol. Microbiol.*, **48**, 1005–1016.
11. Hang,J.Q. and Zhao,G. (2003) Characterization of the 16S rRNA- and membrane-binding domains of Streptococcus pneumoniae Era GTPase: structural and functional implications. *Eur. J. Biochem.*, **270**, 4164–4172.
12. Johnstone,B.H., Handler,A.A., Chao,D.K., Nguyen,V., Smith,M., Ryu,S.Y., Simons,E.L., Anderson,P.E. and Simons,R.W. (1999) The widely conserved Era G-protein contains an RNA-binding domain required for Era function in vivo. *Mol. Microbiol.*, **33**, 1118–1131.
13. Tu,C., Zhou,X., Tropea,J.E., Austin,B.P., Waugh,D.S., Court,D.L. and Ji,X. (2009) Structure of ERA in complex with the 3′ end of 16S rRNA: implications for ribosome biogenesis. *Proc. Natl. Acad. Sci. U.S.A.*, **106**, 14843–14848.
14. Chen,X., Court,D.L. and Ji,X. (1999) Crystal structure of ERA: a GTPase-dependent cell cycle regulator containing an RNA binding motif. *Proc. Natl. Acad. Sci. U.S.A.*, **96**, 8396–8401.
15. Ji,X. (2016) Structural insights into cell cycle control by essential GTPase Era. *Postepy Biochem.*, **62**, 335–342.
16. Sayed,A., Matsuyama,S. and Inouye,M. (1999) Era, an essential Escherichia coli small G-protein, binds to the 30S ribosomal subunit. *Biochem. Biophys. Res. Commun.*, **264**, 51–54.
17. Thurlow,B., Davis,J.H., Leong,V., T,F.M., Williamson,J.R. and Ortega,J. (2016) Binding properties of YjeQ (RsgA), RbfA, RimM and Era to assembly intermediates of the 30S subunit. *Nucleic Acids Res.*, **44**, 9918–9932.
18. Sharma,M.R., Barat,C., Wilson,D.N., Booth,T.M., Kawazoe,M., Hori-Takemoto,C., Shirouzu,M., Yokoyama,S., Fucini,P. and Agrawal,R.K. (2005) Interaction of Era with the 30S ribosomal subunit implications for 30S subunit assembly. *Mol. Cell*, **18**, 319–329.
19. Campbell,T.L. and Brown,E.D. (2008) Genetic interaction screens with ordered overexpression and deletion clone sets implicate the Escherichia coli GTPase YjeQ in late ribosome biogenesis. *J. Bacteriol.*, **190**, 2537–2545.
20. Baba,T., Ara,T., Hasegawa,M., Takai,Y., Okumura,Y., Baba,M., Datsenko,K.A., Tomita,M., Wanner,B.L. and Mori,H. (2006) Construction of Escherichia coli K-12 in-frame, single-gene knockout mutants: the Keio collection. *Mol. Syst. Biol.*, **2**, 2006.0008.
21. Daigle,D.M., Rossi,L., Berghuis,A.M., Aravind,L., Koonin,E.V. and Brown,E.D. (2002) YjeQ, an essential, conserved, uncharacterized protein from Escherichia coli, is an unusual GTPase with circularly permuted G-motifs and marked burst kinetics. *Biochemistry*, **41**, 11109–11117.
22. Razi,A., Guarne,A. and Ortega,J. (2017) The cryo-EM structure of YjeQ bound to the 30S subunit suggests a fidelity checkpoint function for this protein in ribosome assembly. *Proc. Natl. Acad. Sci. U.S.A.*, **114**, E3396–E3403.
23. Campbell,T.L. and Brown,E.D. (2002) Characterization of the depletion of 2-C-methyl-D-erythritol-2,4-cyclodiphosphate synthase in Escherichia coli and Bacillus subtilis. *J.Bacteriol.*, **184**, 5609–5618.
24. Datta,S., Costantino,N. and Court,D.L. (2006) A set of recombineering plasmids for gram-negative bacteria. *Gene*, **379**, 109–115.
25. Bierman,M., Logan,R., O'Brien,K., Seno,E.T., Rao,R.N. and Schoner,B.E. (1992) Plasmid cloning vectors for the conjugal transfer of DNA from Escherichia coli to Streptomyces spp. *Gene*, **116**, 43–49.
26. Datsenko,K.A. and Wanner,B.L. (2000) One-step inactivation of chromosomal genes in Escherichia coli K-12 using PCR products. *Proc. Natl. Acad. Sci. U.S.A.*, **97**, 6640–6645.

27. Link,A.J., Phillips,D. and Church,G.M. (1997) Methods for generating precise deletions and insertions in the genome of wild-type Escherichia coli: application to open reading frame characterization. *J. Bacteriol.*, **179**, 6228–6237.
28. Leong,V., Kent,M., Jomaa,A. and Ortega,J. (2013) Escherichia coli rimM and yjeQ null strains accumulate immature 30S subunits of similar structure and protein complement. *RNA*, **19**, 789–802.
29. Brown,S.D. and Jun,S. (2015) Complete Genome Sequence of Escherichia coli NCM3722. *Genome Announc.*, **3**, e00879-15.
30. Davis,J.H., Tan,Y.Z., Carragher,B., Potter,C.S., Lyumkis,D. and Williamson,J.R. (2016) Modular assembly of the bacterial large ribosomal subunit. *Cell*, **167**, 1610–1622.
31. Jomaa,A., Jain,N., Davis,J.H., Williamson,J.R., Britton,R.A. and Ortega,J. (2014) Functional domains of the 50S subunit mature late in the assembly process. *Nucleic Acids Res.*, **42**, 3419–3435.
32. Eng,J.K., Jahan,T.A. and Hoopmann,M.R. (2013) Comet: an open-source MS/MS sequence database search tool. *Proteomics*, **13**, 22–24.
33. Deutsch,E.W., Shteynberg,D., Lam,H., Sun,Z., Eng,J.K., Carapito,C., von Haller,P.D., Tasman,N., Mendoza,L., Farrah,T. *et al.* (2010) Trans-Proteomic Pipeline supports and improves analysis of electron transfer dissociation data sets. *Proteomics*, **10**, 1190–1195.
34. Shteynberg,D., Deutsch,E.W., Lam,H., Eng,J.K., Sun,Z., Tasman,N., Mendoza,L., Moritz,R.L., Aebersold,R. and Nesvizhskii,A.I. (2011) iProphet: multi-level integrative analysis of shotgun proteomic data improves peptide and protein identification rates and error estimates. *Mol. Cell Proteom.*, **10**, doi:10.1074/mcp.M111.007690.
35. Lam,H., Deutsch,E.W., Eddes,J.S., Eng,J.K., King,N., Stein,S.E. and Aebersold,R. (2007) Development and validation of a spectral library searching method for peptide identification from MS/MS. *Proteomics*, **7**, 655–667.
36. MacLean,B., Tomazela,D.M., Shulman,N., Chambers,M., Finney,G.L., Frewen,B., Kern,R., Tabb,D.L., Liebler,D.C. and MacCoss,M.J. (2010) Skyline: an open source document editor for creating and analyzing targeted proteomics experiments. *Bioinformatics*, **26**, 966–968.
37. Escher,C., Reiter,L., MacLean,B., Ossola,R., Herzog,F., Chilton,J., MacCoss,M.J. and Rinner,O. (2012) Using iRT, a normalized retention time for more targeted measurement of peptides. *Proteomics*, **12**, 1111–1121.
38. Sturn,A., Quackenbush,J. and Trajanoski,Z. (2002) Genesis: cluster analysis of microarray data. *Bioinformatics*, **18**, 207–208.
39. Hao,Y. and Kieft,J.S. (2014) Diverse self-association properties within a family of phage packaging RNAs. *RNA*, **20**, 1759–1774.
40. Hao,Y., Bohon,J., Hulscher,R., Rappe,M.C., Gupta,S., Adilakshmi,T. and Woodson,S.A. (2018) Time-resolved hydroxyl radical footprinting of RNA with X-Rays. *Curr. Protoc. Nucleic Acid Chem.*, **73**, e52.
41. Zheng,S.Q., Palovcak,E., Armache,J.P., Verba,K.A., Cheng,Y. and Agard,D.A. (2017) MotionCor2: anisotropic correction of beam-induced motion for improved cryo-electron microscopy. *Nat. Methods*, **14**, 331–332.
42. Zhang,K. (2016) Gctf: Real-time CTF determination and correction. *J. Struct. Biol.*, **193**, 1–12.
43. Kimanius,D., Forsberg,B.O., Scheres,S.H. and Lindahl,E. (2016) Accelerated cryo-EM structure determination with parallelisation using GPUs in RELION-2. *eLife*, **5**, e18722.
44. Vargas,J., Alvarez-Cabrera,A.L., Marabini,R., Carazo,J.M. and Sorzano,C.O. (2014) Efficient initial volume determination from electron microscopy images of single particles. *Bioinformatics*, **30**, 2891–2898.
45. Tang,G., Peng,L., Baldwin,P.R., Mann,D.S., Jiang,W., Rees,I. and Ludtke,S.J. (2007) EMAN2: an extensible image processing suite for electron microscopy. *J. Struct. Biol.*, **157**, 38–46.
46. Scheres,S.H. (2012) RELION: implementation of a Bayesian approach to cryo-EM structure determination. *J. Struct. Biol.*, **180**, 519–530.
47. Bai,X.C., Rajendra,E., Yang,G., Shi,Y. and Scheres,S.H. (2015) Sampling the conformational space of the catalytic subunit of human gamma-secretase. *eLife*, **4**, e11182.
48. Rosenthal,P.B. and Henderson,R. (2003) Optimal determination of particle orientation, absolute hand, and contrast loss in single-particle electron cryomicroscopy. *J. Mol. Biol.*, **333**, 721–745.
49. Pettersen,E.F., Goddard,T.D., Huang,C.C., Couch,G.S., Greenblatt,D.M., Meng,E.C. and Ferrin,T.E. (2004) UCSF Chimera–a visualization system for exploratory research and analysis. *J. Comput. Chem.*, **25**, 1605–1612.
50. Terwilliger,T.C., Sobolev,O.V., Afonine,P.V. and Adams,P.D. (2018) Automated map sharpening by maximization of detail and connectivity. *Acta Crystallogr. D Struct. Biol.*, **74**, 545–559.
51. Adams,P.D., Afonine,P.V., Bunkoczi,G., Chen,V.B., Davis,I.W., Echols,N., Headd,J.J., Hung,L.W., Kapral,G.J., Grosse-Kunstleve,R.W. *et al.* (2010) PHENIX: a comprehensive Python-based system for macromolecular structure solution. *Acta Crystallogr. D Biol. Crystallogr.*, **66**, 213–221.
52. Afonine,P.V., Poon,B.K., Read,R.J., Sobolev,O.V., Terwilliger,T.C., Urzhumtsev,A. and Adams,P.D. (2018) Real-space refinement in PHENIX for cryo-EM and crystallography. *Acta Crystallogr. D Struct. Biol.*, **74**, 531–544.
53. Emsley,P. and Cowtan,K. (2004) Coot: model-building tools for molecular graphics. *Accta Crystallogr. D Biol. Crystallogr.*, **60**, 2126–2132.
54. Emsley,P., Lohkamp,B., Scott,W.G. and Cowtan,K. (2010) Features and development of Coot. *Accta Crystallogr. D Biol. Crystallogr.*, **66**, 486–501.
55. Himeno,H., Hanawa-Suetsugu,K., Kimura,T., Takagi,K., Sugiyama,W., Shirata,S., Mikami,T., Odagiri,F., Osanai,Y., Watanabe,D. *et al.* (2004) A novel GTPase activated by the small subunit of ribosome. *Nucleic Acids Res.*, **32**, 5303–5309.
56. Guo,Q., Goto,S., Chen,Y., Feng,B., Xu,Y., Muto,A., Himeno,H., Deng,H., Lei,J. and Gao,N. (2013) Dissecting the in vivo assembly of the 30S ribosomal subunit reveals the role of RimM and general features of the assembly process. *Nucleic Acids Res.*, **41**, 2609–2620.
57. Traub,P. and Nomura,M. (1968) Structure and function of Escherichia coli ribosomes. I. Partial fractionation of the functionally active ribosomal proteins and reconstitution of artificial subribosomal particles. *J. Mol. Biol.*, **34**, 575–593.
58. Traub,P. and Nomura,M. (1969) Structure and function of Escherichia coli ribosomes. VI. Mechanism of assembly of 30 s ribosomes studied in vitro. *J. Mol. Biol.*, **40**, 391–413.
59. Traub,P. and Nomura,M. (1969) Studies on the assembly of ribosomes in vitro. *Cold Spring Harb. Symp. Quant. Biol.*, **34**, 63–67.
60. Schuwirth,B.S., Borovinskaya,M.A., Hau,C.W., Zhang,W., Vila-Sanjurjo,A., Holton,J.M. and Cate,J.H. (2005) Structures of the bacterial ribosome at 3.5 A resolution. *Science*, **310**, 827–834.
61. Lauber,M.A., Rappsilber,J. and Reilly,J.P. (2012) Dynamics of ribosomal protein S1 on a bacterial ribosome with cross-linking and mass spectrometry. *Mol. Cell Proteom.*, **11**, 1965–1976.
62. Powers,T. and Noller,H.F. (1990) Dominant lethal mutations in a conserved loop in 16S rRNA. *Proc. Natl. Acad. Sci. U.S.A.*, **87**, 1042–1046.
63. Sashital,D.G., Greeman,C.A., Lyumkis,D., Potter,C.S., Carragher,B. and Williamson,J.R. (2014) A combined quantitative mass spectrometry and electron microscopy analysis of ribosomal 30S subunit assembly in E. coli. *eLife*, **3**, e04491.
64. Mulder,A.M., Yoshioka,C., Beck,A.H., Bunner,A.E., Milligan,R.A., Potter,C.S., Carragher,B. and Williamson,J.R. (2010) Visualizing ribosome biogenesis: parallel assembly pathways for the 30S subunit. *Science*, **330**, 673–677.
65. Besancon,W. and Wagner,R. (1999) Characterization of transient RNA-RNA interactions important for the facilitated structure formation of bacterial ribosomal 16S RNA. *Nucleic Acids Res.*, **27**, 4353–4362.
66. Sykes,M.T. and Williamson,J.R. (2009) A complex assembly landscape for the 30S ribosomal subunit. *Annu. Rev. Biophys.*, **38**, 197–215.
67. Adilakshmi,T., Bellur,D.L. and Woodson,S.A. (2008) Concurrent nucleation of 16S folding and induced fit in 30S ribosome assembly. *Nature*, **455**, 1268–1272.
68. Karbstein,K. (2013) Quality control mechanisms during ribosome maturation. *Trends Cell Biol.*, **23**, 242–250.
69. Strunk,B.S., Loucks,C.R., Su,M., Vashisth,H., Cheng,S., Schilling,J., Brooks,C.L. 3rd, Karbstein,K. and Skiniotis,G. (2011) Ribosome assembly factors prevent premature translation initiation by 40S assembly intermediates. *Science*, **333**, 1449–1453.

70. Strunk,B.S., Novak,M.N., Young,C.L. and Karbstein,K. (2012) A translation-like cycle is a quality control checkpoint for maturing 40S ribosome subunits. *Cell*, **150**, 111–121.
71. Lopez-Alonso,J.P., Kaminishi,T., Kikuchi,T., Hirata,Y., Iturrioz,I., Dhimole,N., Schedlbauer,A., Hase,Y., Goto,S., Kurita,D. *et al.* (2017) RsgA couples the maturation state of the 30S ribosomal decoding center to activation of its GTPase pocket. *Nucleic Acids Res.*, **45**, 6945–6959.
72. Jomaa,A., Stewart,G., Mears,J.A., Kireeva,I., Brown,E.D. and Ortega,J. (2011) Cryo-electron microscopy structure of the 30S subunit in complex with the YjeQ biogenesis factor. *RNA*, **17**, 2026–2038.
73. Guo,Q., Yuan,Y., Xu,Y., Feng,B., Liu,L., Chen,K., Sun,M., Yang,Z., Lei,J. and Gao,N. (2011) Structural basis for the function of a small GTPase RsgA on the 30S ribosomal subunit maturation revealed by cryoelectron microscopy. *Proc. Natl. Acad. Sci. U.S.A.*, **108**, 13100–13105.
74. Jomaa,A., Stewart,G., Martin-Benito,J., Zielke,R., Campbell,T.L., Maddock,J.R., Brown,E.D. and Ortega,J. (2011) Understanding ribosome assembly: the structure of in vivo assembled immature 30S subunits revealed by cryo-electron microscopy. *RNA*, **17**, 697–709.
75. Yang,Z., Guo,Q., Goto,S., Chen,Y., Li,N., Yan,K., Zhang,Y., Muto,A., Deng,H., Himeno,H. *et al.* (2014) Structural insights into the assembly of the 30S ribosomal subunit in vivo: functional role of S5 and location of the 17S rRNA precursor sequence. *Protein Cell*, **5**, 394–407.
76. Ni,X., Davis,J.H., Jain,N., Razi,A., Benlekbir,S., McArthur,A.G., Rubinstein,J.L., Britton,R.A., Williamson,J.R. and Ortega,J. (2016) YphC and YsxC GTPases assist the maturation of the central protuberance, GTPase associated region and functional core of the 50S ribosomal subunit. *Nucleic Acids Res.*, **44**, 8442–8455.
77. Clatterbuck Soper,S.F., Dator,R.P., Limbach,P.A. and Woodson,S.A. (2013) In vivo X-ray footprinting of pre-30S ribosomes reveals chaperone-dependent remodeling of late assembly intermediates. *Mol. Cell*, **52**, 506–516.
78. Prossliner,T., Skovbo Winther,K., Sorensen,M.A. and Gerdes,K. (2018) Ribosome Hibernation. *Annu. Rev. Genet.*, **52**, 321–348.
79. Basu,A. and Yap,M.N. (2017) Disassembly of the Staphylococcus aureus hibernating 100S ribosome by an evolutionarily conserved GTPase. *Proc. Natl. Acad. Sci. U.S.A.*, **114**, E8165–E8173.
80. Zundel,M.A., Basturea,G.N. and Deutscher,M.P. (2009) Initiation of ribosome degradation during starvation in Escherichia coli. *RNA*, **15**, 977–983.
81. Lu,Q. and Inouye,M. (1998) The gene for 16S rRNA methyltransferase (ksgA) functions as a multicopy suppressor for a cold-sensitive mutant of era, an essential RAS-like GTP-binding protein in Escherichia coli. *J. Bacteriol.*, **180**, 5243–5246.
82. Datta,P.P., Wilson,D.N., Kawazoe,M., Swami,N.K., Kaminishi,T., Sharma,M.R., Booth,T.M., Takemoto,C., Fucini,P., Yokoyama,S. *et al.* (2007) Structural aspects of RbfA action during small ribosomal subunit assembly. *Mol. Cell*, **28**, 434–445.
83. Ghosal,A., Babu,V.M.P. and Walker,G.C. (2018) Elevated levels of Era GTPase improve growth, 16S rRNA processing, and 70S ribosome assembly of escherichia coli lacking highly conserved multifunctional YbeY endoribonuclease. *J. Bacteriol.*, **200**, e00278-18.